Final Report for AOARD 08-4004

Vertical alignment of single-walled carbon nanotubes on nanostructure fabricated by atomic force microscope

Date: December 16, 2009

Name of Principal Investigators: Haiwon Lee
- e-mail address : haiwon@hanyang.ac.kr
- Institution : Department of Chemistry, Hanyang University
- Mailing Address : 17 Haengdang-dong, Seongdong-gu, Seoul 133-791, Korea
- Phone : +82-2-2220-0945
- Fax : +82-2-2296-0287

Period of Performance: 10/03/2008 – 09/03/2009

Abstract

Our work has been concentrated on both the selective formation of single-walled carbon nanotubes (SWCNTs) on a surface-modified Si substrate with functional groups, and the fabrication of SWCNT-three-dimensional networks (SWCNT-3DNs) on complex 3D-structured templates including deep pores and high pillars. In order to grow SWCNTs on a surface-modified Si substrate selectively, a micro-contact printing and a low energy proton beam irradiation were applied, respectively. Field electron emission properties of self-aligned MWCNT-SWCNT hetero-line patterns were also studied. The SWCNT-3DNs were successfully fabricated inside the deep pores of a porous silicon structure as well as over the micro-sized Si pillar arrays on Si substrate.

Introduction

The single-walled carbon nanotubes (SWCNTs) were directly synthesized on the silicon (Si) or silicon oxide (SiO_2) substrates for fabricating the SWCNTs-based electronic devices and optoelectronics, and the desired density, areal selectivity, and directional controllability are quite important for the synthesis of SWCNTs. It is also critical to have uniform synthesis of high-purity SWCNTs with desired position, density, and direction on the three-dimensional (3D) complex structures on Si or SiO_2 substrates. Electronic devices in future are expected to have a complex 3D structure in order to increase the density of their integration. By forming the catalyst on a substrate selectively, it is possible to grow CNTs on the substrate selectively. Therefore, many approaches have been tried to form metal catalysts onto the Si substrate selectively by lithographic lift-off, soft lithography, offset printing, or micro-contact printing (μCP). The μCP has attracted much attention due to its simplicity, low cost, and easily scaled up process. Low-energy ion beam irradiation has been used for surface modification of substrates because of its potential capability to change mechanical, chemical, and physical properties of materials. Therefore, the low-energy ion beam irradiation can be used for the selective growth of CNTs by forming catalyst selectively on Si substrate. Suspension of SWCNTs between two electrodes is of interest both academically and practically. Several groups have reported the synthesis of suspended CNTs on patterned Si or SiO_2 substrates for applications such as channels or connecting wires in electronic

Report Documentation Page

Form Approved
OMB No. 0704-0188

1. REPORT DATE	2. REPORT TYPE	3. DATES COVERED
04 JAN 2010	**FInal**	**03-10-2008 to 03-09-2009**

4. TITLE AND SUBTITLE
Vertical alignment of single-walled carbon nanotubes on nanostructure fabricated by atomic force microscope

5a. CONTRACT NUMBER
FA48690814004

5b. GRANT NUMBER

5c. PROGRAM ELEMENT NUMBER

6. AUTHOR(S)
Haiwon Lee

5d. PROJECT NUMBER

5e. TASK NUMBER

5f. WORK UNIT NUMBER

7. PERFORMING ORGANIZATION NAME(S) AND ADDRESS(ES)
Hanyang University,Haengdang-dong, Seongdong-gu,Seoul 133-791,Korea (South),KR,133791

8. PERFORMING ORGANIZATION REPORT NUMBER
N/A

9. SPONSORING/MONITORING AGENCY NAME(S) AND ADDRESS(ES)
AOARD, UNIT 45002, APO, AP, 96337-5002

10. SPONSOR/MONITOR'S ACRONYM(S)
AOARD

11. SPONSOR/MONITOR'S REPORT NUMBER(S)
AOARD-084004

12. DISTRIBUTION/AVAILABILITY STATEMENT
Approved for public release; distribution unlimited

13. SUPPLEMENTARY NOTES

14. ABSTRACT
The current work has been concentrated on both the selective formation of single-walled carbon nanotubes (SWCNTs) on a surface-modified Si substrate with functional groups, and the fabrication of SWCNT-three-dimensional networks (SWCNT-3DNs) on complex 3D-structured templates including deep pores and high pillars. In order to grow SWCNTs on a surface-modified Si substrate selectively, a micro-contact printing and a low energy proton beam irradiation were applied, respectively. Field electron emission properties of self-aligned MWCNT-SWCNT hetero-line patterns were also studied. The SWCNT-3DNs were successfully fabricated inside the deep pores of a porous silicon structure as well as over the micro-sized Si pillar arrays on Si substrate.

15. SUBJECT TERMS
Nanotechnology, Carbon nano tubes

16. SECURITY CLASSIFICATION OF:			17. LIMITATION OF ABSTRACT	18. NUMBER OF PAGES	19a. NAME OF RESPONSIBLE PERSON
a. REPORT	b. ABSTRACT	c. THIS PAGE			
unclassified	**unclassified**	**unclassified**	**Same as Report (SAR)**	**52**	

devices. For the synthesis of the high-density SWCNTs on a complex 3D structured substrate, the catalysts should be uniformly dispersed onto the surface of substrates.

Experiment

1. Preparation of Fe-Mo catalyst solution

An Fe-Mo bimetallic catalyst solution was prepared by ultrasonication for 30 min using an ethanol solvent, $Fe(NO_3)_3 \cdot 9H_2O$ (Junsei), and a Mo solution (ICP/DCP standard solution, Aldrich). The molar ratio of Fe/Mo in the catalyst solution was 4/1.

2. Selective adsorption of metal catalysts on Si substrates using micro-contact printing

Figure 1 is the experimental scheme of patterning octadecyltrichlorosilane (OTS) stripes on a Si substrate through micro-contact printing (μCP). Briefly, a polydimethylsiloxane (PDMS) solution was poured onto the surface of the master Si substrate (Figure 1(a)). After 24 h, the PDMS mold was prepared by removing hardened PDMS from the master Si substrate. Figure 2 and Figure 3 showed that the PDMS mold had a clear stripe pattern that was transferred from the master Si substrate.

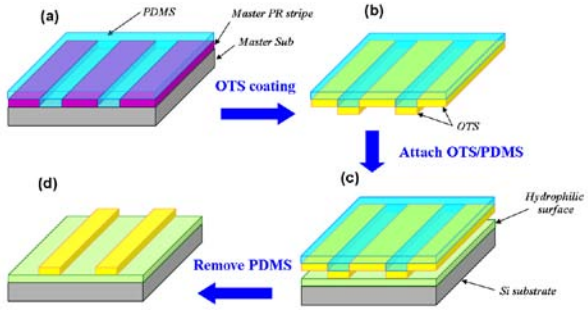

Figure 1. Schematics for the fabrication process of OTS stripes on Si substrate by μCP.

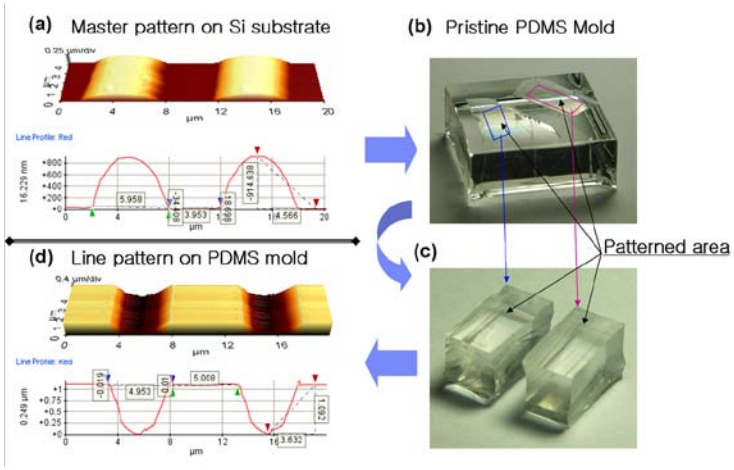

Figure 2. (a) AFM image of master pattern on the master Si substrate. (b and c) Optical images of the Pristine PDMS mold. (d) AFM image of the stripes pattern on the pristine PDMS mold.

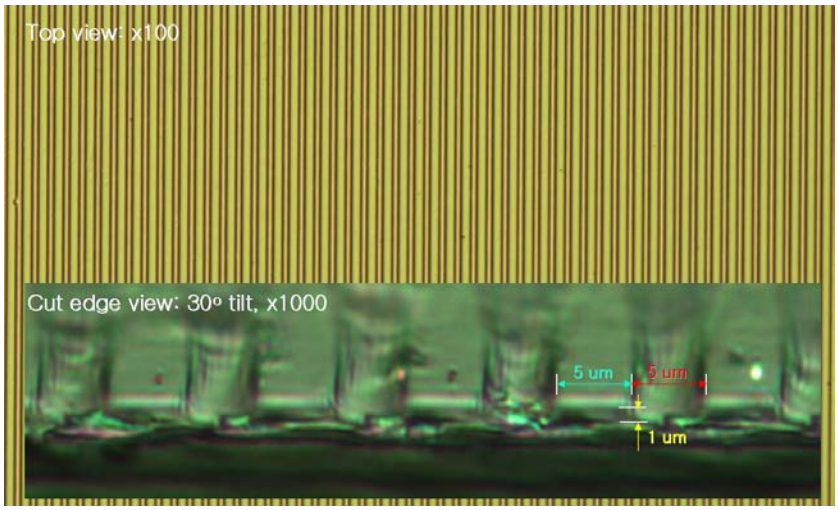

Figure 3. Optical microscope images of line patterns on the pristine PDMS mold. The inset is enlarged image.

In order to form an OTS monolayer onto the surface of the PDMS mold, diluted OTS solution (3 mM in Toluene) was spin-coated onto the PDMS mold (Figure 1(b)). Then the OTS-coated PDMS (OTS/PDMS) mold was attached onto the modified Si substrate with hydroxyl groups. At that time, piranha treatment of the Si substrate was performed to modify the surface of the Si substrate with hydroxyl groups. After 10 seconds of attachment, the OTS/PDMS mold was detached from the Si substrate so that the OTS stripe was formed on the surface of the Si substrate, as described in Figure 1(c and d). The Si substrate coated with OTS stripe is referred to as the OTS-stripe/Si substrate.

To form a catalyst onto the OTS-stripe/Si substrate, the OTS-stripe/Si substrate was soaked in the Fe-Mo(4/1)/ethanol catalyst solution for 10 minutes (Figure 4(a)). By rinsing the substrate fully after the soaking process, Fe-Mo catalyst stripes were formed on the OTS-stripe/Si substrate. At this time, the Fe-Mo catalyst adhered only on the hydroxyl area of the OTS-stripe/Si substrate (Figure 4(b)).

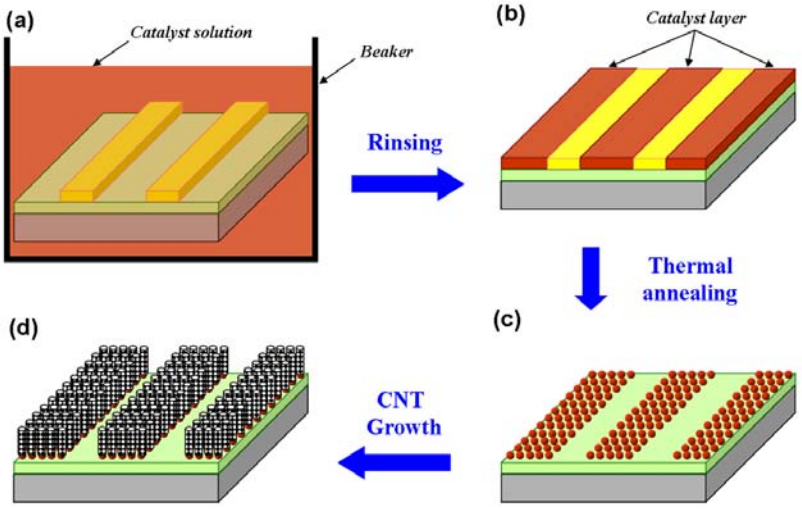

Figure 4. Schematics for the fabrication process of catalyst stripes for the selective synthesis of CNTs on a substrate.

3. Selective adsorption of metal catalysts on Si substrates using low-energy proton beam irradiation.

Figure 5 shows the experimental process for the selective modification of a silicon substrate using nanosphere lithography. A polystyrene (PS) nanosphere array was placed onto the silicon substrate by the drop-coating method using 20 μl of the nanosphere solution diluted by mixing with a solution of methanol and DI water (Fig. 5a). A 3 keV low-energy proton beam with a fluence of 1×10^{16} ions/cm^2 was irradiated onto the silicon substrate in a high-vacuum chamber with a base pressure of 1.5×10^{-6} Torr (Fig. 5b). After irradiation with the proton beam, the PS nanospheres were removed using THF solvent (Fig. 5c). The substrate was treated with a 1.0% HF solution diluted with DI water (Fig. 5d). The height variation of the silicon oxide layer after HF treatment was measured using atomic force microscopy (AFM) (Nanoscope IIIa, Digital Instruments, CA). AFM was operated in the tapping mode with Al backside-coated silicon tips, which had a resonance frequency of 320 kHz and a radius curvature of less than 10 nm (Nanoworld). Composition of the silicon oxide layer on the substrate was determined by auger electron spectroscopy (AES) (PHI 680 Auger Nanoprobe, Physical Electronics.) AES was performed under an electron beam at 10 kV and 10 nA. The water contact angle on the silicon surface was measured using a KRÜSS model FM 40 goniometer with various functional groups including Si-OH, Si-H, Si-O-Si, and Si-O-Pr. The Si-OH functional group was generated by treatment with a piranha solution (H_2O_2:H_2SO_4 = 3:7 v/v %). The Si-H surface group was generated on the silicon substrate by treatment with the HF solution. The Si-O-Si surface functional groups of the native oxide layer were cleaned with acetone, IPA, and DI water. The Si-O-Pr is a virtual surface functional group of the silicon oxide layer formed by the proton beam.

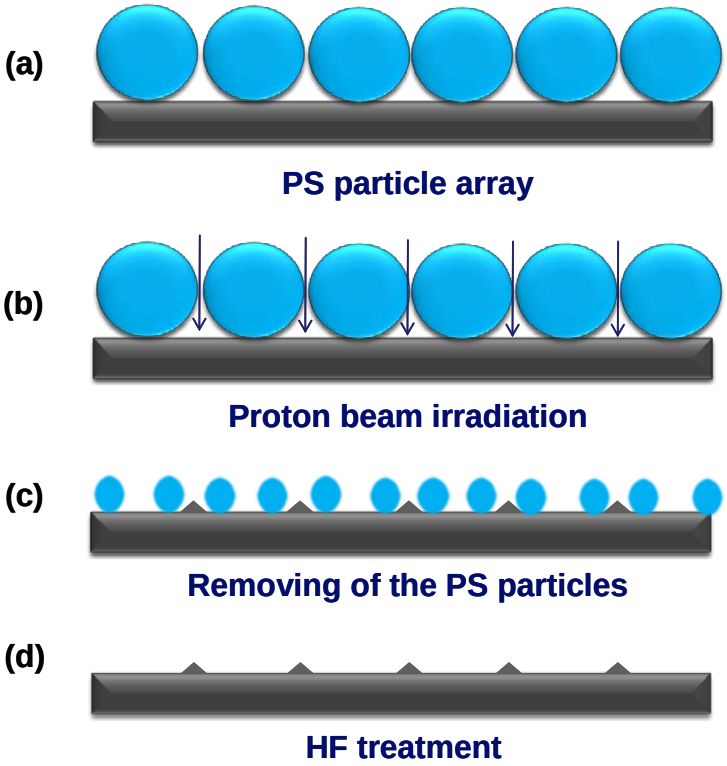

Figure 5. The fabrication process of silicon structures by using both nanosphere lithography and proton beam irradiation.

Figure 6 shows the experimental process for fabricating the oxide pattern for the selective growth of CNTs. The proton beam was directly irradiated onto the silicon substrate, which was covered with a shadow mask as shown in Figs. 6a and 6b. The beam-irradiated substrate was treated with a HF solution as previously described (Figs. 6c and 6d). The HF-treated substrate coated with the silicon oxide pattern was immersed in a 0.01M Fe-Mo bimetallic catalyst solution in ethanol for two hr. The Fe-Mo particles adsorbed to the more hydrophilic surface (Fig. 6e). The catalyst-adsorbed substrates were inserted into the center of a quartz tube reactor. And the SWCNTs were selectively synthesized on the proton beam-irradiated area of a Si substrate.

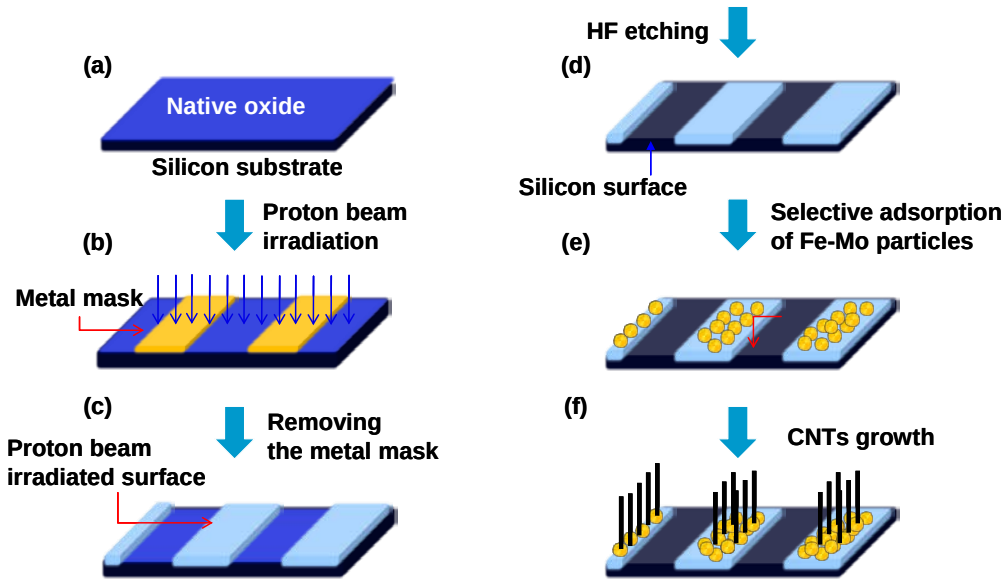

Figure 6. Fabrication of the silicon patterns for the selective growth of CNTs.

4. Adsorption of metal catalysts inside the pores of a porous silicon substrate.

A porous silicon layer was fabricated on the surface of a silicon wafer using a common electrochemical etching technique. Briefly, an n-type silicon (100) wafer was placed into a mixture of HF and ethanol solvent. Then, a porous silicon layer with complex pores (diameter of 200 – 1,000 nm and depth of ~ 40 μm) was formed (Figs. 7a-c) by applying a DC voltage with a white light (white halogen lamp; 50 W) for 40 min. The porous silicon substrate was cleaned by ultrasonication in acetone, ethanol, and deionized water (DI water) sequentially.

The as-prepared porous silicon substrate was cleaned and modified with hydroxyl group by socking it into Piranha solution (H_2SO_4:H_2O_2=3:1) for 30 min. The porous silicon substrate was then washed by ultrasonication in DI water to remove the piranha solution from the pores. The surface morphologies of both the top and inner surface of the pores were very rough (Figs. 7c and d).

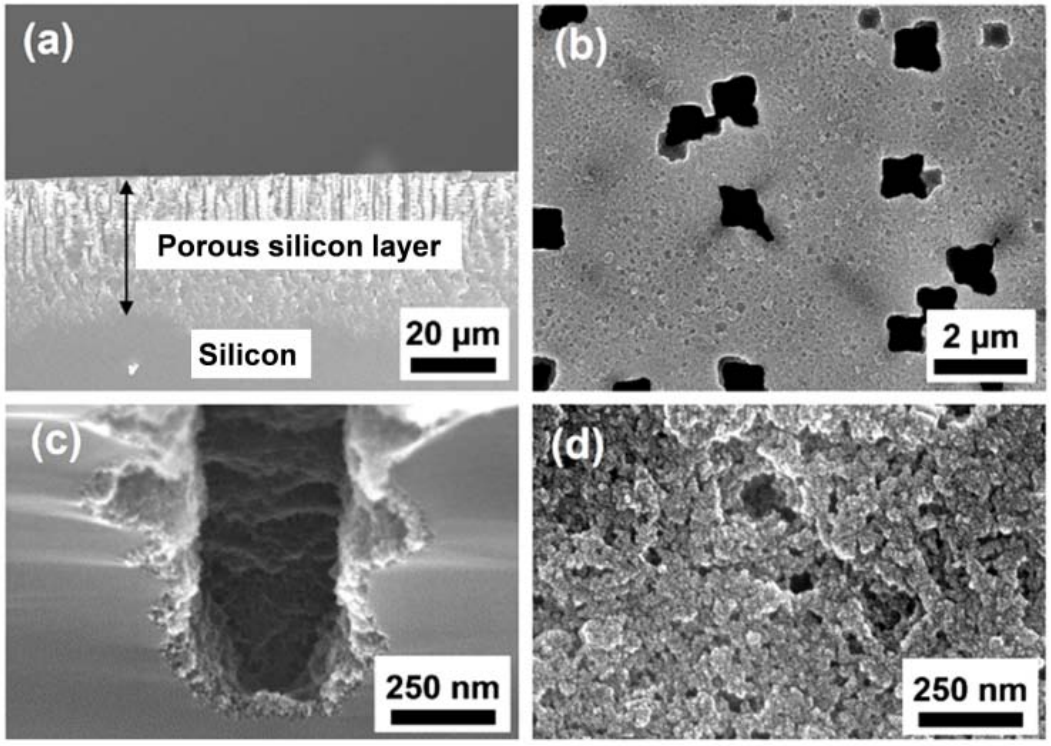

Figure 7. SEM images of the pristine porous silicon substrate: (a) Cut edge, (b) Top surface, (c) Bottom of a pore, and (d) Enlarged top surface.

To deposit the Fe-Mo bimetallic catalyst on the inner wall surface of the pores of the porous silicon substrate, the substrate was soaked in the Fe-Mo catalyst solution for 20 minutes with ultrasonication, and then washed thoroughly in ethanol solvent several times. Catalyst solution was dispersed uniformly on the whole area of porous silicon substrate including the bottom of deep pores by applying an ultrasonication during the dipping process. The density of catalyst nanoparticles was controlled by adjusting the concentration of "Fe" in ethanol solvent. In this study, the concentration of "Fe" was 10 mM.

5. Adsorption of metal catalysts on Si pillar arrays.

Figure 8 shows the experimental procedure for the fabrication of SWCNT-3DNs. The Si pillar array (Fig. 8a) was fabricated on a highly doped n-type Si (100) substrate by using a general photolithography technique which included a deep Si etching process (SLR-770-10R-B, Plasma Therm Co.). The diameter and the height of the prepared Si pillar are 1.0 μm and 21.0 μm, respectively. These dimensions correspond to a Si pillar aspect ratio of 21. The gaps between two neighboring Si pillars are 1.0 μm (small gap) and 1.8 μm (large gap). The surface of the pillar/Si substrate was cleaned and modified with hydroxyl groups by a piranha treatment. The surface-modified pillar/Si substrate was soaked in the Fe-Mo catalyst solution for 30 minutes (Fig. 8b), and then fully rinsed with ethanol. As a result, Fe-Mo catalyst nanoparticles were uniformly formed on the entire surface area of the Si pillar arrays (Fig. 8c). The synthesis of SWCNTs was conducted in a horizontal quartz tube reactor using low pressure thermal chemical vapor deposition (LPTCVD).

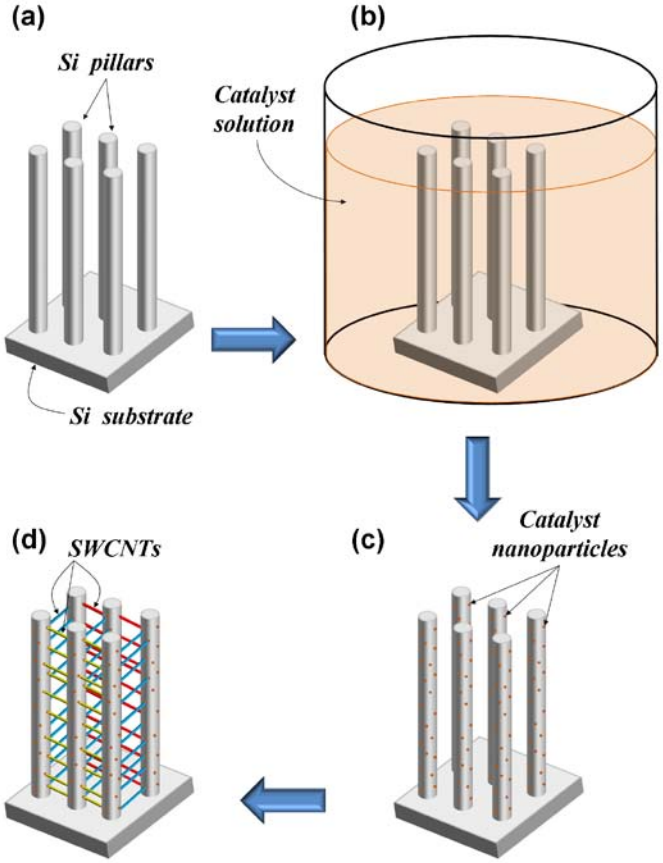

Figure 8. Schematic illustrations of the procedures for the fabrication of SWCNT-3DNs on a dense Si pillar array having a high aspect ratio.

6. Synthesis of SWCNTs using LP-TCVD.

SWCNTs were synthesized in a horizontal quartz tube reactor. The diameter and the length of the reactor are 40 and 800 mm, respectively. The catalyst-formed porous silicon substrate was annealed at 400°C for 30 min in ambient air. Subsequently, the reactor was pumped down to 9.0 x 10^{-3} torr and heated to 800°C. When the temperature of the reactor reached 800°C, 300 sccm of NH_3 gas was introduced into the reactor for 10 min to reduce the iron oxide to the iron catalyst. After the NH_3 pretreatment, 10 sccm of C_2H_2 gas was introduced for 10 min to synthesize SWCNTs while maintaining a pressure of 3.3 x 10^{-1} torr. Finally, the reactor was cooled down to room temperature under a pressure of 9.0 x 10^{-3} torr.

7. Characterization of SWCNTs

Scanning electron microscope (SEM: S-4700, Hitachi; and S-4800, Hitachi) was used to characterize the catalysts and the CNTs such as density and morphology. Atomic force microscope (AFM: Nanoscope 3a, Digital Instruments) was used to image the OTS stripe and the Fe-Mo catalyst nanoparticles formed on substrates. Raman spectroscopy (LabRam HR, 514 nm laser excitation wavelength, Jobin-Yvon; NRS-3000, 532 nm laser excitation wavelength, Jasco; Nanofinder-30, 488 nm and 633 nm laser excitation wavelengths, Tokyo Instruments Co.) was used to investigate the diameter distribution, the crystallinity, and the

metallicity of SWCNTs. Transmission electron microscope (TEM: TECNAI-F20, 200 keV, Philips; TECNAI-F30 S-Twin, 300 keV, Philips) was used to characterize the structure and crystallinity of CNTs. A diode-type home-made field electron emission analyzer was used to investigate the field electron emission properties of the selectively grown CNTs on the Si substrate.

Results and Discussions

1. Fabrication of self-aligned MWCNT-SWCNT hetero-line patterns on Si substrates by using both micro-contact printing and field electron emission

Figure 9 shows the AFM topography image and a height profile of OTS-stripe patterns transferred from the OTS/PDMS mold (line widths of stripe: 7 μm, pattern space: 3 μm) through μCP. They clearly show that the OTS-stripes were formed on the Si substrate with 7 μm line widths, 3 μm line spaces, and ~1.2 nm height. Figure 9(a) shows that the OTS-stripes have many defects, which implies that our technique for patterning OTS using μCP is not good. Many residual clusters formed on the whole area of the OTS-stripe/Si substrate are the Si particles and dust attached during the sampling process.

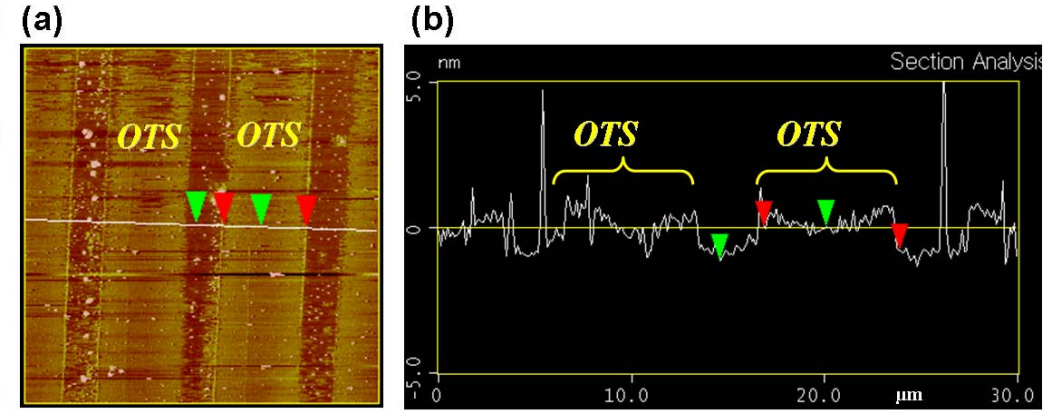

Figure 9. AFM image (a) and height profile (b) of OTS-stripe patterns formed on Si substrate by μCP.

Figure 10 shows that the Fe-Mo catalyst nanoparticles were formed on the hydroxyl groups with high density. The line width, line space, and height of the Fe-Mo catalyst were 3 μm, 7 μm, and ~ 40 nm, respectively. On the other hand, the Fe-Mo catalyst was also formed on the OTS-stripe area with low density, and because of that the OTS-stripes formed by μCP have many defects, as shown in Figure 9.

Figure10(c and d) show the enlarged AFM topographic image and height profile of the Fe-Mo catalyst stripe patterns. They revealed that the Fe-Mo catalyst were agglomerated and formed larger-sized clusters on the Si substrate. This catalyst agglomeration resulted in the growth of MWCNTs instead of SWCNTs, as shown in Figure 12. Figure 11 show the enlarged AFM topography image and height profile of the Fe-Mo catalyst formed on an OTS-stripe area. This figure reveals that many of the Fe-Mo nanoparticles with small sizes, under 1.3 nm, were formed on the defects of the OTS.

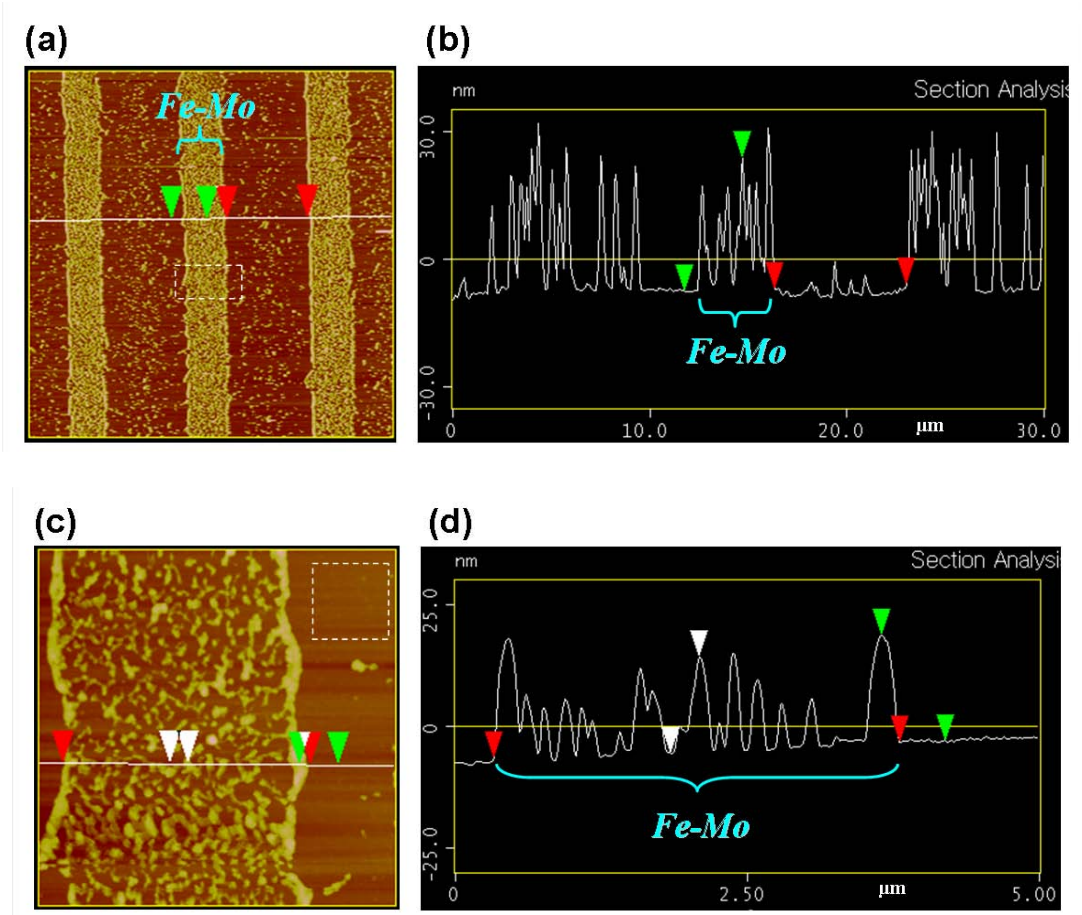

Figure 10. AFM images (a and c) and height profiles (b and d) of Fe-Mo catalyst stripe patterns deposited on the Si substrate by a dipping method.

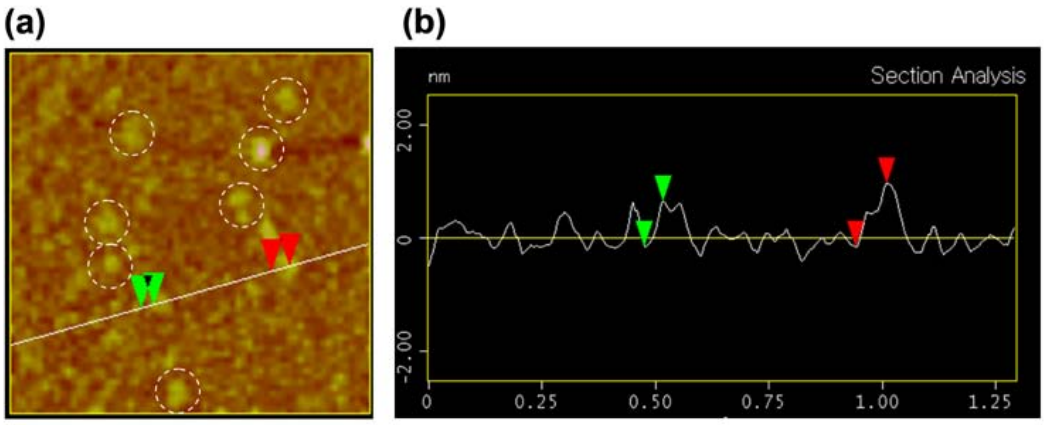

Figure 11. Enlarged AFM image (a) and height profile (b) of Fe-Mo catalyst nanoparticles deposited on the defect site of the OTS-stripe area.

Figure 12 shows the SEM images of CNTs grown on the Fe-Mo/OTS-stripe/Si substrate by thermal decomposition of C_2H_2 at 800 °C for 10 minutes. They reveal that the MWCNTs having high density were grown on the Fe-Mo stripe area having 3 μm of line width (corresponding with a hydroxyl group area), and few SWCNTs were found between the MWCNTs. On the OTS-stripe area (7 μm of line width), few MWCNTs and many SWCNTs were grown with low-density. This large amount of SWCNTs was owing to the small-sized catalyst nanoparticles formed on the OTS-stripe area as shown in Figure 11.

Figure 13 shows the field electron emission characteristics measured from the vertically grown CNT stripe by fabricating a diode structure including Cu anode and CNT cathode. It shows stable field electron emission property during four time measurements. The turn-on field is 4 V/μm at the 10 μA/cm^2, and the current density is high at 1 mA/cm^2 at 8V/um. These results imply that the vertically grown CNT stripe can be used to vacuum electronic devices as a field electron emitter with high efficiency.

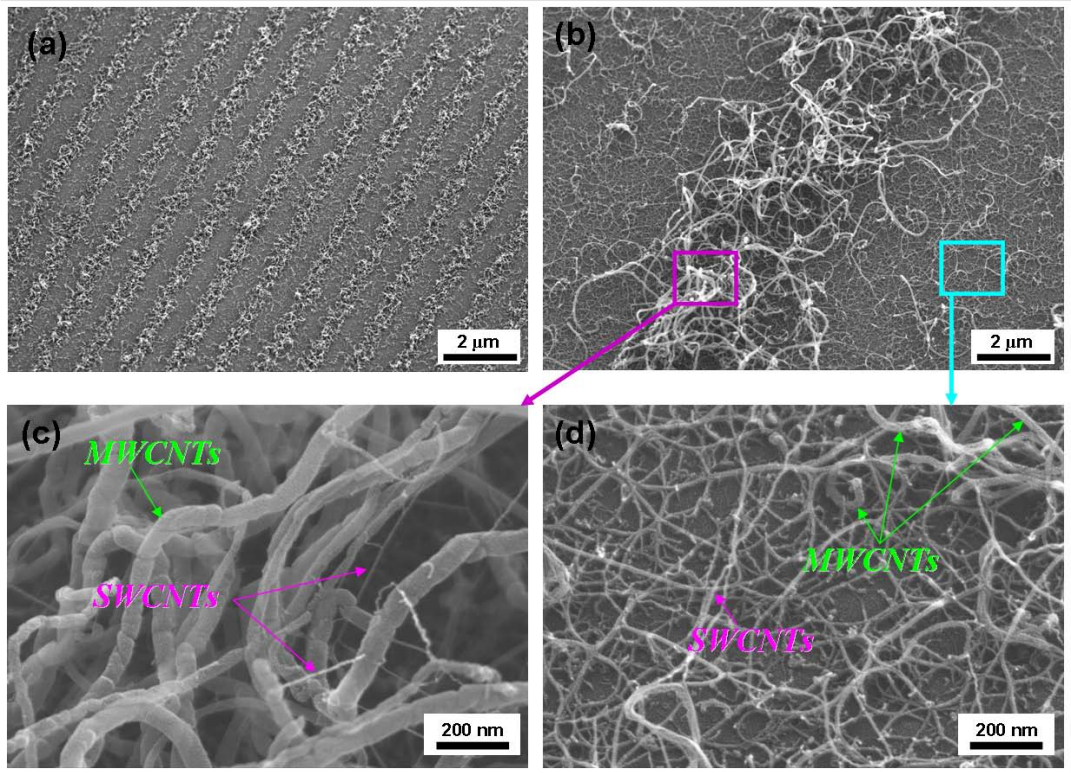

Figure 12. SEM images of CNTs synthesized on the Fe-Mo deposited Si substrate. Enlarged views of the CNTs synthesized on the Fe-Mo stripe pattern area (a) and on the Fe-Mo catalyst nanoparticles deposited on the defects of the OTS-stripe area.

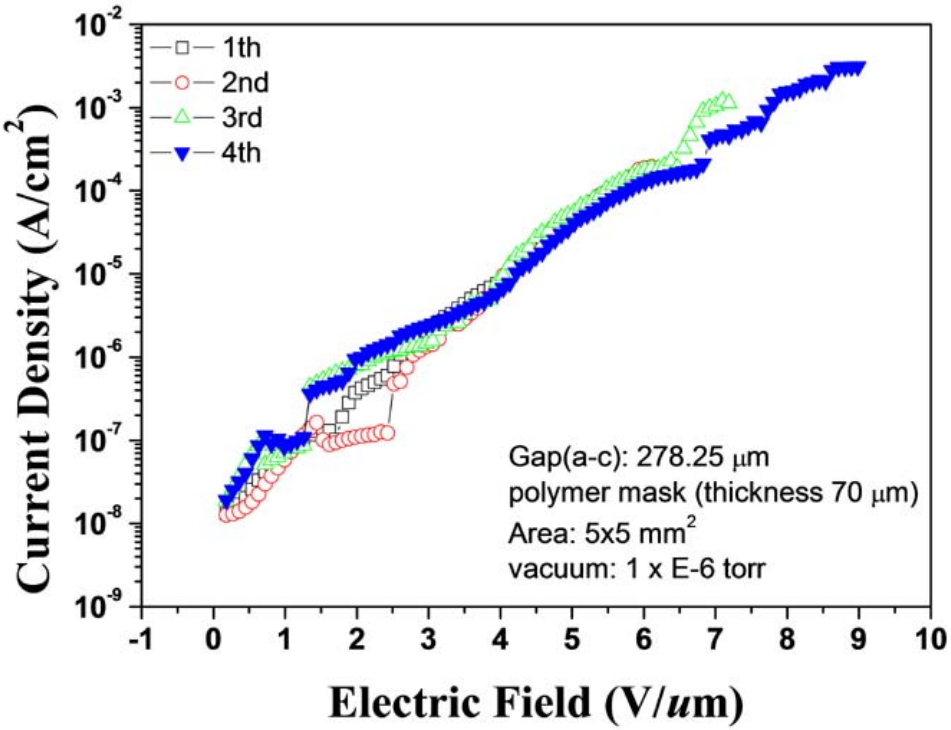

Figure 13. Field emission properties of protruded CNTs stripe synthesized on the Fe-Mo deposited Si substrate.

In summary, the selective growth of CNTs on a Si substrate was also performed by using both micro-contact printing and dipping methods. The Fe-Mo catalyst was well adsorbed with high density on the hydrophilic surface of the OTS-stripe/Si substrate. Some Fe-Mo catalysts were also adsorbed on the OTS-stripe area due to the defects of the OTS-stripe. MWCNTs were grown in greater volume than SWCNTs on the Fe-Mo catalysts due to the metal agglomeration of iron at a high temperature (800 °C). Field emission properties of CNT stripe were investigated, which show low a turn-on field (4 V/um at the 10 μA/cm^2) and a high current density of 1 mA/cm^2 at 8 V/um, which can be used for vacuum electronics as an electron emitter. For the selective growth of SWCNTs on a Si substrate, more systematical studies are required.

2. Growth of SWCNTs on the line-patterned Si template modified by using low-energy proton beam irradiation

Figure 14 shows AFM images of the silicon oxide pattern produced by proton beam irradiation and the height of oxide dots according to etch time with HF. After removal of the PS nanospheres, the polymer ring pattern remained in the center of the hexagonal oxide dot configuration (Fig. 14a). This pattern was a result of the scattered proton beam affecting the PS nanospheres through a radical reaction with the polycyclic structure. The polymer rings were cleared by HF treatment as shown in Fig. 14b. Figure 14c shows height variations in the silicon oxide dots according to the total HF etch time of the native oxide layer. The height variation of the silicon oxide dots was saturated at about 15 Å, which is the thickness of the native oxide layer on a bare silicon substrate. This indicates that the native oxide layer

was removed by the HF solution, but the silicon oxide formed by the proton beam was not influenced by the HF treatment. Also, the silicon oxide dots had a strikingly different structure relative to that of the native oxide.

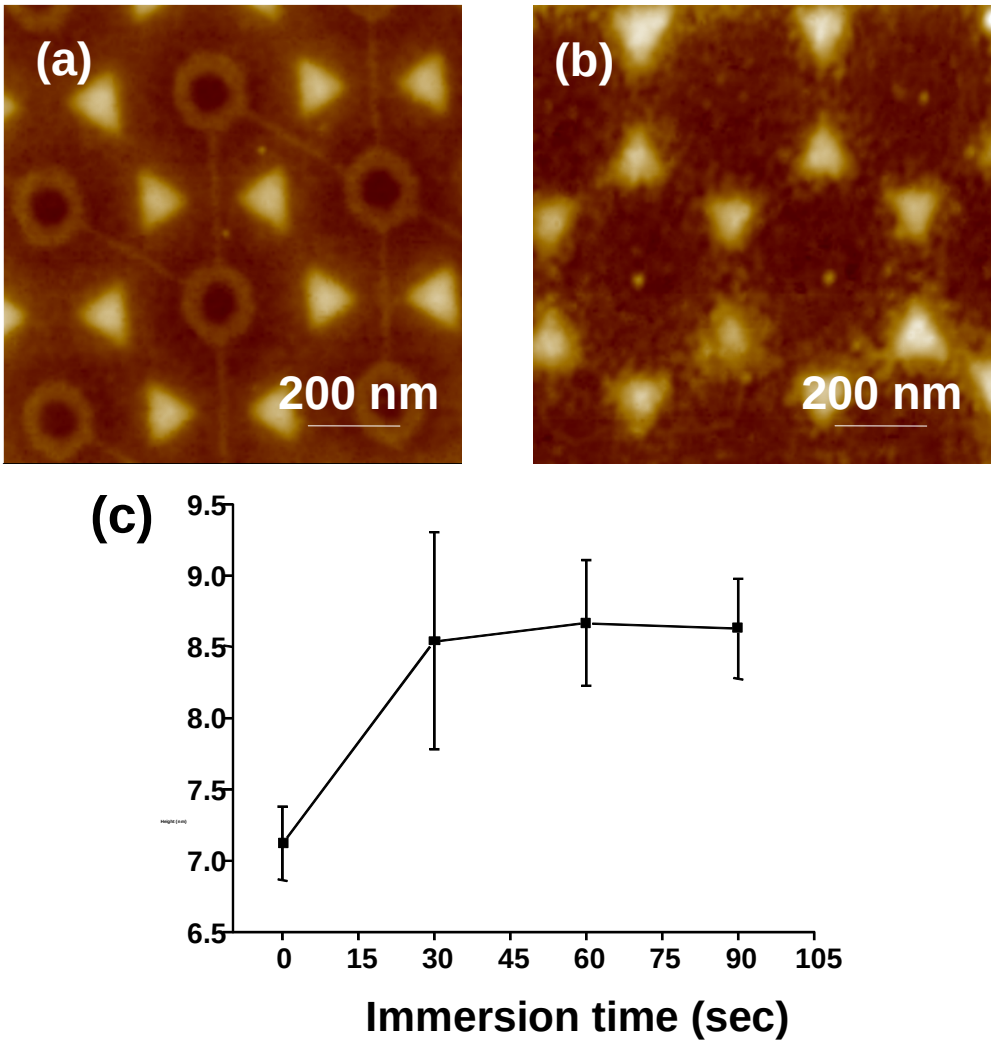

Figure 14. AFM images of silicon oxide structures fabricated by proton beam irradiation using a PS array; (a) after removal of the PS nanospheres and (b) after HF treatment. (c) The height of the silicon oxide layer vs. HF etch time of the native oxide layer.

Figure 15 shows the auger depth profiles of the bare silicon and proton-beam irradiated silicon substrates. The initial atomic ratio of oxygen for the bare silicon substrate was 50%; however, the atomic ratio of oxygen for the proton-beam irradiated silicon substrate was higher than that of the bare silicon. This indicates that the proton beam caused damage to the Si–Si chemical bond, and that the resulting unstable Si atoms reacted with oxygen either from the ambient water or air, to form a more stable chemical state. Oxygen was detected to about 30 Å and 60 Å depths on the bare silicon and proton-beam irradiated silicon substrates, respectively (Fig. 14). This indicates that the proton beam penetrated through the silicon substrate, allowing the oxygen to diffuse into the damaged silicon layer.

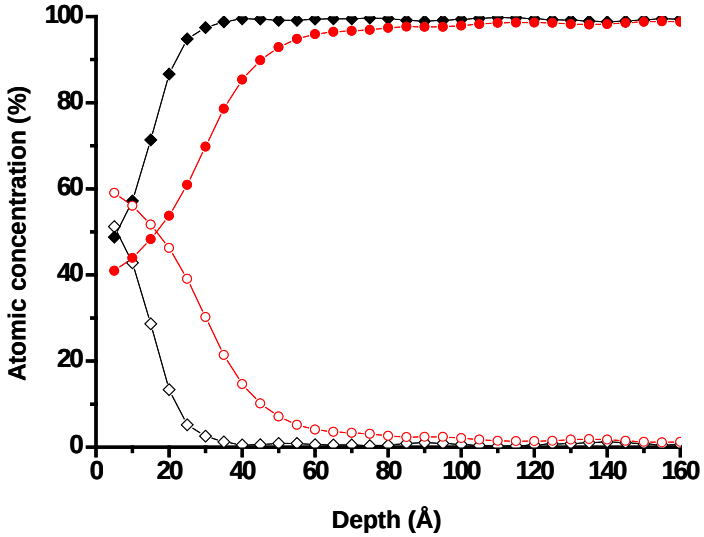

Figure 15. AES depth profiles of the bare silicon substrate (-◆- and -◇-) and the proton-beam irradiated silicon substrate (-●- and -○-). Profile data for two components of silicon (-◆-and-●-) and oxygen (-◇- and -○-) on the sample are shown.

The physical property of the surface was characterized by measuring the water contact angles on both silicon surfaces. Figure 16 shows the values of the water contact angles on the four surfaces. The water contact angle of the Si-OH modified surface was below 7°, due to the extreme hydrophilic property of this surface. The mean contact angle between the water and the Si-O-Si was about 28°. After removing the native oxide by HF treatment, the water contact angle of the Si-H surface was increased to about 80°, which is comparable to the contact angle of 68° measured on the Si-O-Pr surface. These data indicate that the Si-O-Pr-modified surface is more hydrophilic than the Si-H surface, and that the physical properties between the Si-O-Si and Si-O-Pr surfaces are different.

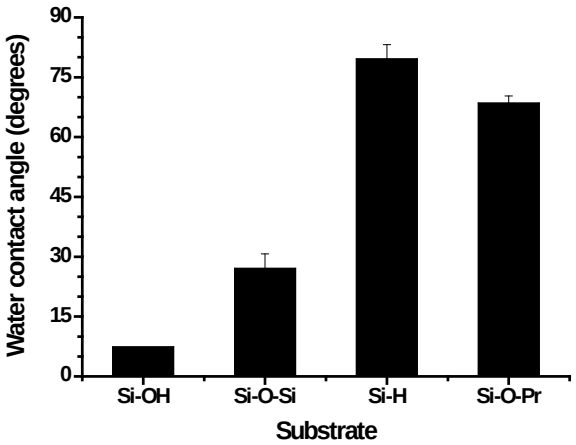

Figure 16. Water contact angles for various silicon surfaces.

Figure 17 shows the AFM images of the Fe-Mo adsorbed surfaces of both the silicon oxide layer and the bare silicon surface. The density of Fe-Mo particles on the silicon oxide layer was higher than that on the silicon surface because the adsorption of metal ions depends upon the hydrophilic or hydrophobic property of the surface.

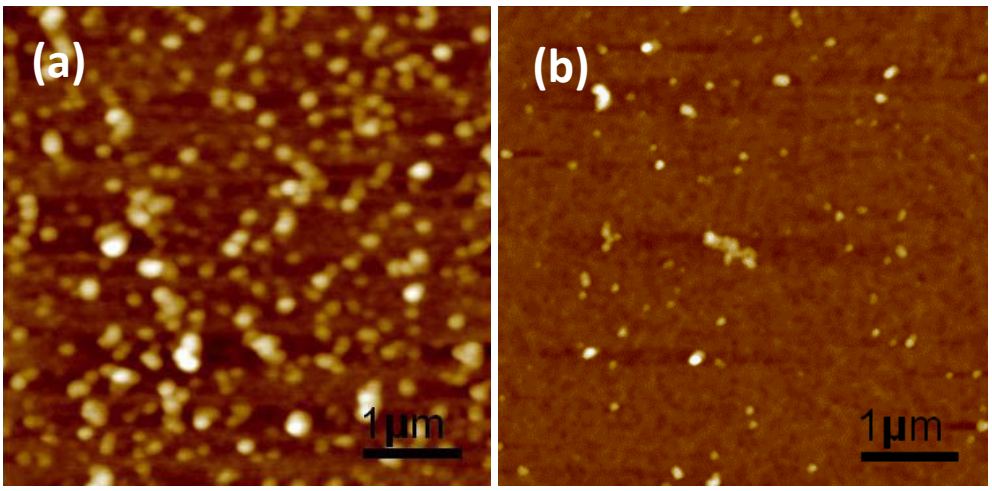

Figure 17. AFM images after Fe-Mo adsorption onto a substrate with a silicon oxide pattern; (a) silicon oxide and (b) silicon surface.

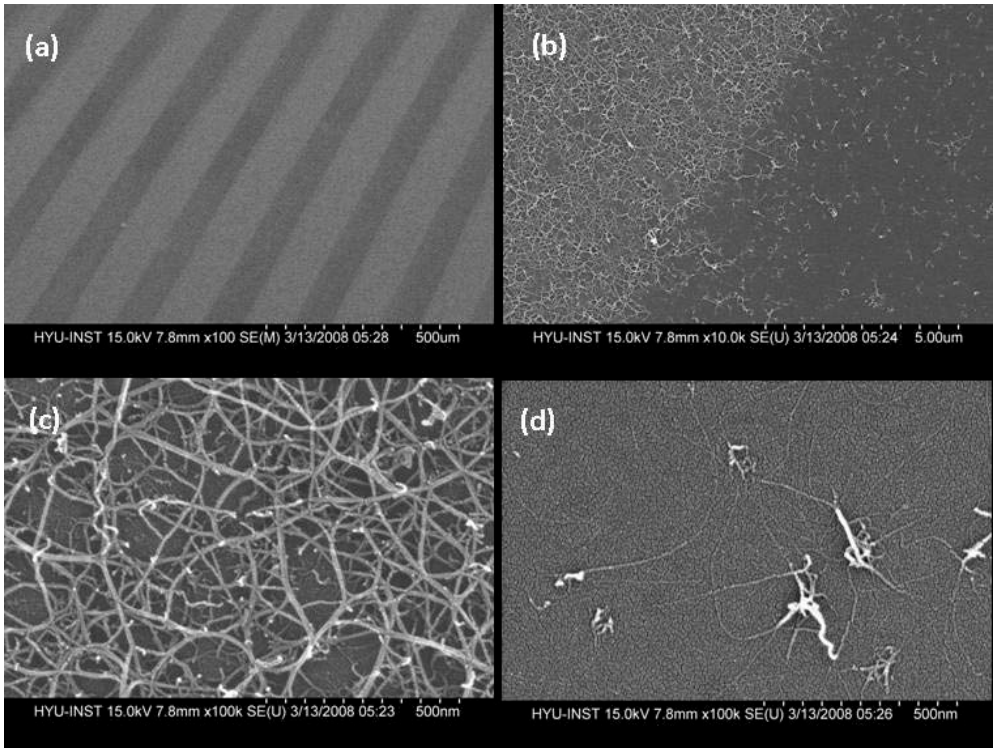

Figure 18. SEM images after growth of CNTs on the silicon oxide pattern; (a) silicon oxide pattern before CNT growth, (b) interface image between the silicon oxide layer and the silicon surface after CNT growth. Enlarged images of CNTs on the (c) silicon oxide layer and (d) silicon surface.

Figure 18a shows SEM images of the oxide patterns. The pitch of the pattern was 200 μm, which consisted of the 50 μm between the oxide patterns (dark area) and the pattern width of 150 μm (bright area). The SEM image of selectively grown CNTs was obtained at the interface between the silicon oxide layer and silicon surface as shown in Fig. 18b. The density of CNTs on the silicon oxide layer was higher than that of the silicon surface because the density of CNTs depends on the number of Fe-Mo particles. Enlarged images of CNTs on the silicon oxide layer (Fig 18c) and on the silicon surface (Fig 18d) are shown.

In summary, we demonstrated a basic technique for using low-energy ion beam lithography to modify a silicon substrate. The silicon substrate was partially modified by proton beam irradiation using a shadow mask. The chemical etching process for removing the native oxide did not affect the silicon oxide layer formed by the proton beam, which had a different surface property than the base silicon surface. Also, the lower water contact angle was obtained on the Si-O-Pr surface than the native silicon oxide removed silicon substrate. The Fe-Mo bimetallic catalysts were well adsorbed onto the Si-O-Pr modified silicon oxide layer, preparing them for growth of CNTs. CNTs were selectively grown on the silicon oxide patterned substrate.

3. Fabrication of SWCNT-3DNs inside the pores of a porous silicon structure

The rough surface morphology of the pristine porous silicon substrate prevented us from imaging catalyst nanoparticles formed either on the inner wall surface of the pores or on the top surface of the porous silicon substrate. To evaluate the formation of catalyst nanoparticles on the silicon surface, we deposited the catalyst nanoparticles on a planar silicon substrate instead of on the porous silicon substrate using the same dipping conditions. The catalyst nanoparticles deposited on a planar silicon substrate by the dipping method are shown in Fig. 19. The roughness and the average particle height of the catalysts were 1.8 and 7.6 nm, respectively. It should be noted that the inner wall surface of the pores is different from that of planar silicon, therefore the population of catalyst nanoparticles would differ between these two different substrates. Nevertheless, SEM images of SWCNTs shown in Fig. 20 imply that the catalyst nanoparticles were also formed both on the top surface and inside the pores of a porous silicon substrate.

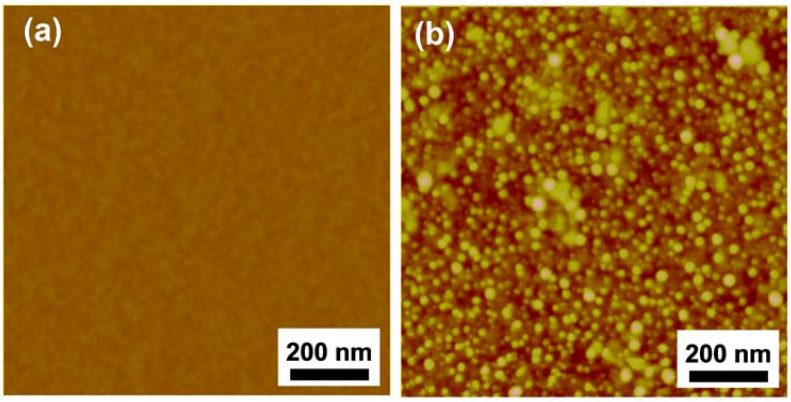

Figure 19. AFM images of (a) a planar silicon substrate, and (b) catalyst nanoparticles formed on a planar silicon substrate by dipping method.

SEM images of the as-synthesized SWCNTs formed on a porous silicon substrate by thermal decomposition of C_2H_2 at 800°C for 10 min are shown in Fig. 20. Most SWCNTs synthesized on the top surface had a noodle-like shape and formed two-dimensional network along the top surface (Fig. 20b). The SWCNTs inside the pores were not only synthesized along the inner wall surfaces of the pores but also spanned it with various shapes and directions, resulting in the SWCNT-3DNs (Figs. 20c-d). SEM analysis also revealed that the SWCNT-3DNs were formed throughout the pores without multi-walled carbon nanotubes. This implies that uniform catalyst nanoparticles were deposited throughout the inner wall surface of the pores by the dipping method.

Figure 21 shows that the SWCNTs made "**Y**"-shaped contacts in 3D space, forming a SWCNT 3-D network. It is likely that the SWCNT-3DN is the outcome of both the simple chaotic overgrowth of SWCNTs in a confined space under thermal vibration, and van der Waals interactions between the SWCNTs. It should be noted that we could not directly estimate the diameter of either an individual SWCNT or a bundle of SWCNTs in SEM images because a single-line of CNT shown in SEM image (i.e. Fig 21) can be either a single SWCNT or a bundle of SWCNTs as shown in Fig. 22

TEM analysis revealed that the as-synthesized SWCNTs are either an individual SWCNT or a bundle of SWCNTs with various diameters (Figs. 22a-b). The SWCNTs have a clean surface, and good crystallinity. Figure 6c clearly shows that the "**Y**"-shaped contacts of the SWCNT-3DN were made up by van der Waals interactions between SWCNTs.

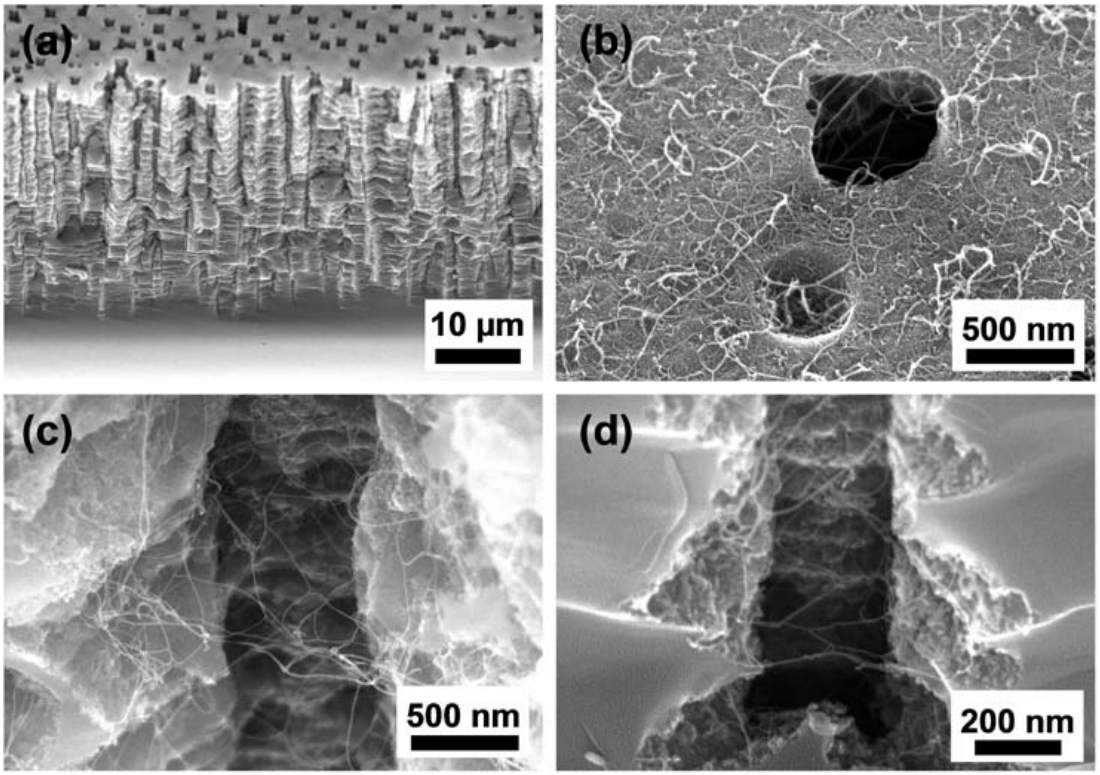

Figure 20. SEM images of SWCNTs synthesized on a porous silicon substrate: (a) Cut edge under low magnification, (b) Top surface, (c) Middle area of a pore, and (d) Bottom area of a pore.

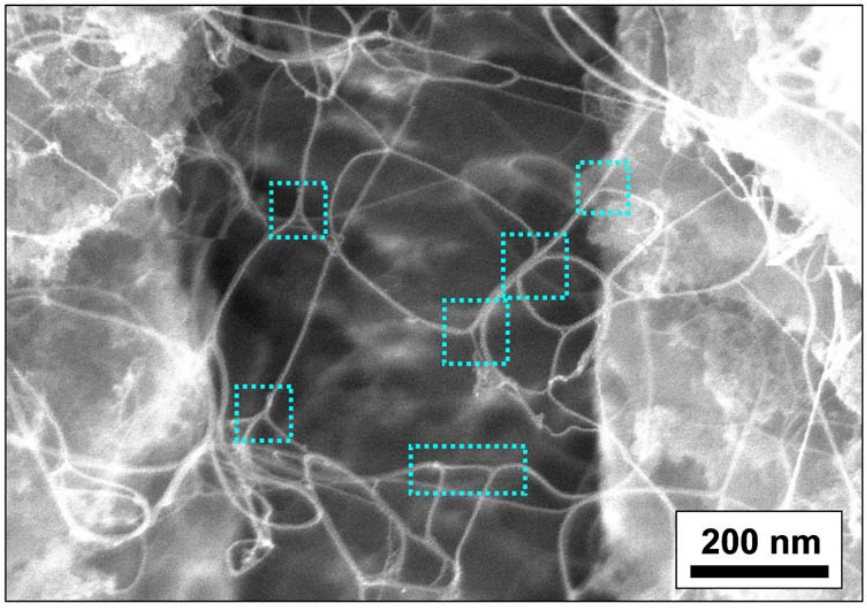

Figure 21. Magnified SEM image of the SWCNT-3DNs synthesized in the pore of a porous silicon substrate. The squares drawn with a dotted line indicate the joints of the SWCNT networks.

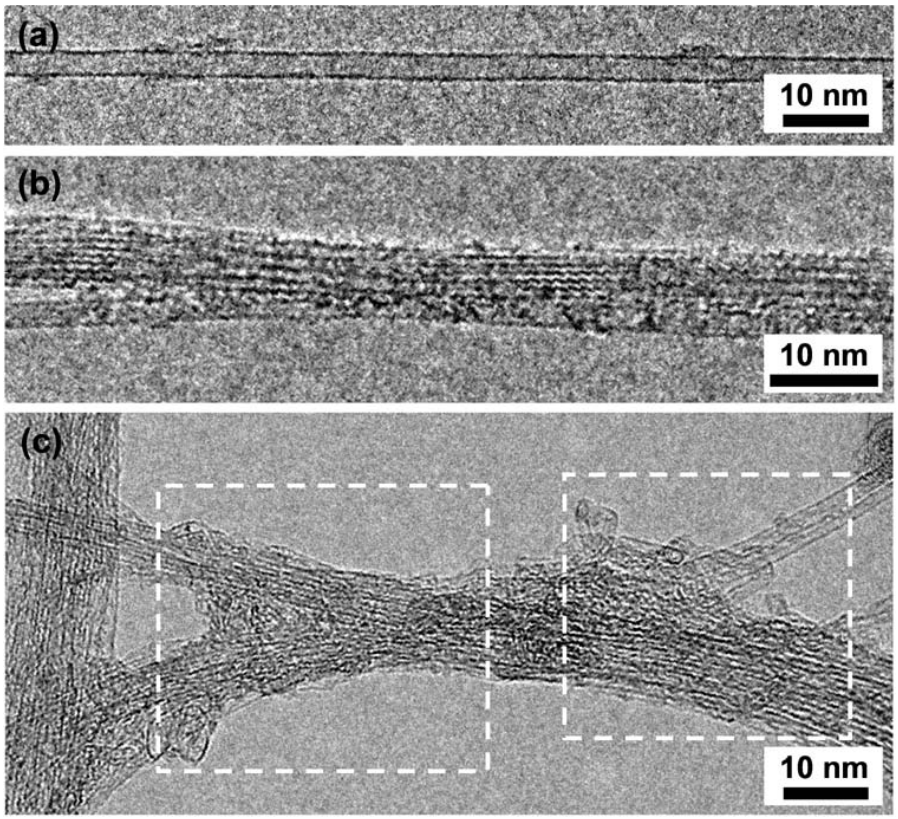

Fig. 22. TEM images of (a) an individual SWCNT, (b) a bundle of SWCNTs, and (c) a SWCNT network synthesized in the pores of a porous silicon substrate. The squares drawn with a dotted line indicate the joints of the SWCNT network.

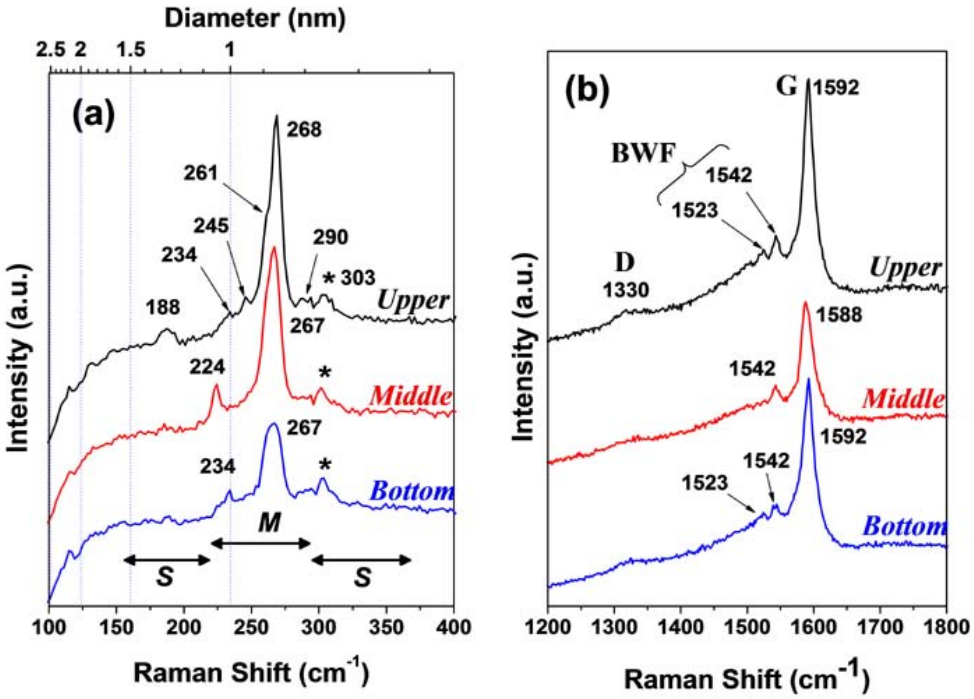

Figure 23. Raman spectra of the SWCNT-3DNs synthesized in different areas (such as upper, middle, and bottom areas) of a pore: (a) RBM frequency range, and (b) G and D frequency range. The wavelength of the excitation laser was 514 nm.

Raman spectra of the SWCNT 3-D networks synthesized in different areas of a pore are shown in Fig. 23. The diameter of SWCNTs was calculated by applying the formula, $d^{0.93}$ (nm) = $238/\nu_{RBM}$ (cm^{-1}), where ν_{RBM} is the radial breathing mode (RBM) frequency and d is the diameter of the SWCNT. The assignments of metallic (***M***) and semi-conducting (***S***) SWCNTs indexed in Fig. 23a are based on a Kataura plot. Clear RBMs at 100-300 cm^{-1}, a weak D-band at 1,330 cm^{-1}, clear Breit-Wigner-Fano (BWF)- bands at 1,523-1,542 cm^{-1}, and a sharp G-band at 1,588-1,592 cm^{-1} are evident in the Raman spectra. These findings imply that the SWCNTs were synthesized throughout the pores. The weak intensity of the D-bands indicates that the SWCNTs had good crystallinity. The shapes of the RBMs (Fig. 23a) indicate that metallic SWCNTs with small diameters (about 0.8-1.1 nm) were synthesized inside the pores. Consistent with this, BWF peaks at 1,523 and 1,542 cm^{-1}, corresponding to metallic SWCNTs, were clearly visible (Fig. 23b). Although the Raman spectra of SWCNTs show a single strong peak in RBM frequency range throughout the pore, it is not directly indicating that most SWCNTs have uniform diameter of 0.87 nm (corresponding at 268 cm^{-1}) as revealed in TEM analysis (Fig. 22).

In summary, The SWCNT-3DNs were first fabricated inside the pores of a porous silicon substrate by thermal decomposition of C_2H_2 at 800°C. A dipping method combined with ultrasonication was good for the formation of uniform catalyst nanoparticles on the inner wall surface throughout the pores. The SWCNTs inside the pores were not only synthesized along the inner wall surfaces of the pores but also spanned it with various shapes and directions, resulting in the SWCNT-3DNs. SEM, TEM, and Raman analysis showed that the SWCNTs have a clean surface and a good crystallinity. It was also revealed that the SWCNT-3DNs were made up by bundling between SWCNTs. Our findings will inform the fabrication of nano-sized filters or sensing channels for application in future microfluidic chips.

4. Fabrication of high-density SWCNT-3DNs on Si pillar arrays

Figure 24(a-d) shows the SEM images of the SWCNTs synthesized on the dense Si pillar array. The SWCNTs were synthesized not only along the Si pillar surface, but also across the 3D space between neighboring Si pillars. Most suspended SWCNTs were formed between neighboring Si pillars with a small gap, and a few of them were formed between two Si pillars with a large gap (Figure 24b). The directional formation phenomenon of SWCNTs that develops between neighboring Si pillars has been explained as the combination of the geometrical effect of the pillar structure and the thermal vibration effect of the SWCNTs. It was also shown that the SWCNTs have a 3D network structure, not only through the Si pillar array (Figure 24b), but also through connections with each other in 3D space (Figure 24c). This arrangement is due to the overgrowth of SWCNTs and the van der Waals interactions between SWCNTs. Figure 1d clearly indicates that the suspended SWCNTs formed on the entire 3D space between the Si pillars over their entire length. This result implies that the catalyst nanoparticles were formed on the entire surface area of the dense Si pillar array by the dipping method. TEM analysis (Figure 24e) revealed that the SWCNTs have a bundle structure, and the SWCNTs are connected to each other by bundling in 3D space, which corresponds with the SEM image(Figure 24c).

Based on the SEM analysis, the average number of suspended SWCNTs between two neighboring Si pillars (having a small gap) was calculated at 101 ± 9 ea. By defining the unit cell (dotted square in Figure 24b; the area of a unit cell is 8 μm^2) of the SWCNT-3DNs /Si pillar array, the average density of suspended SWCNTs is given by $D = 4 \times N / 8$ (ea/μm^2), where D is the average density of suspended SWCNTs and N is the average number of suspended SWCNTs between two neighboring Si pillars having a small gap. As a result, the average density of the suspended SWCNTs synthesized between the Si pillars was calculated at 50.5 ea/μm^2.

In summary, we have synthesized high-density SWCNT-3DNs on a dense Si pillar array having a high aspect ratio. Utilizing the dipping method within a Fe-Mo/ethanol solution resulted in the uniform formation of catalyst nanoparticles on the entire surface area of the dense Si pillar array. The suspended SWCNTs have a 3D network structure not only through the Si pillar arrays but also by bundling each other in 3D space. The average number of suspended SWCNTs between two close Si pillars (gap is 1.0 μm) was 101 ± 9 ea, so that the average density of suspended SWCNTs was 50.5 ea/μm^2. This result will be useful for the application of future electronics and energy alternatives as a highly efficient nano-electrode by having both an ultra-large active surface area and high conductivity.

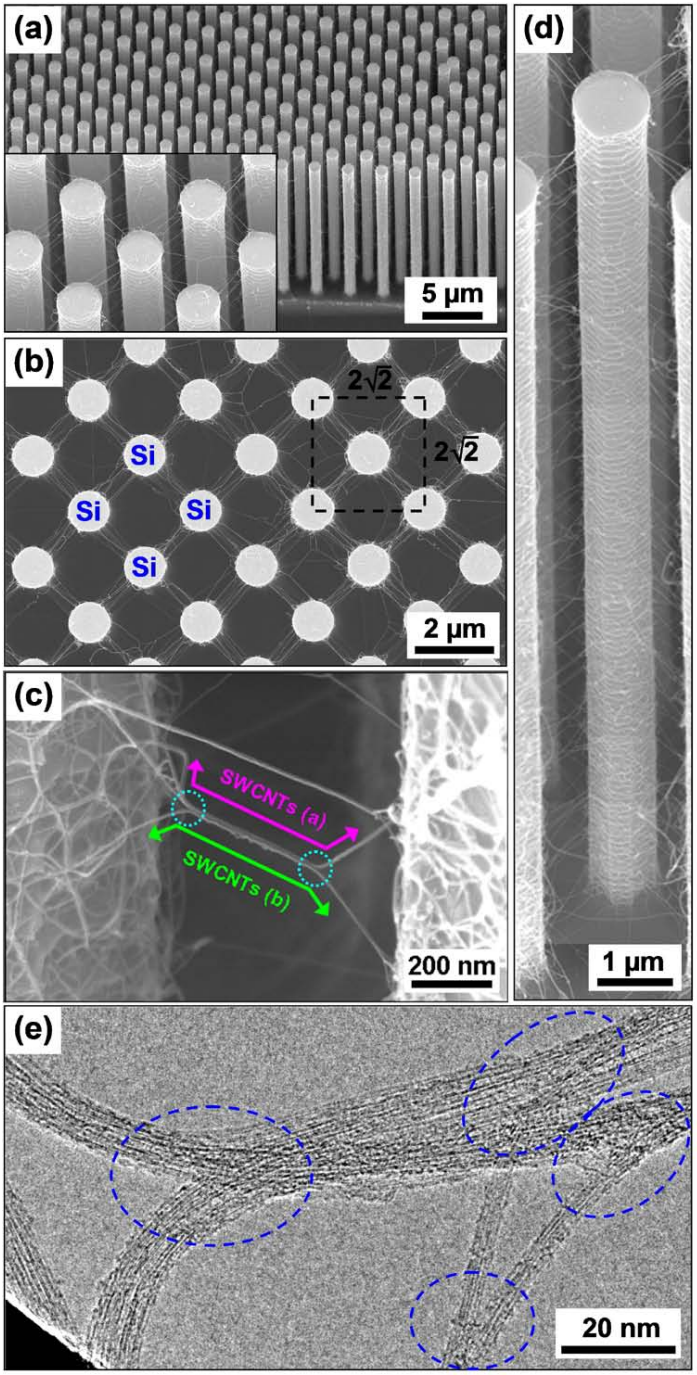

Figure 24. SEM images (a-d) and TEM image (e) of the SWCNT-3DNs synthesized between the dense Si pillar array; (a) tilted view with 30°, (b) top view, (c) enlarged side view of the 3-D SWCNT-networks, (d) enlarged side view of one Si pillar with a tilted angle of 30°. The inset in (a) is an enlarged SEM image of (a). Dotted square in (b) indicates the unit-cell of the SWCNTs/Si pillar array. Dotted circles in (c) and (e) indicate the connecting point of the SWCNT-3DNs, respectively.

List of Publications

1. Publications (SCI Papers)

[1] Tae Jae LEE, Jeongeun SEO, Haiwon Lee, “Vertically aligned growth of single-walled carbon nanotubes on an Fe-Mo/MgO/Si substrate prepared by using a dipping method combined with an UV-ozone treatment”, J. Korean Phys Soc. 53 (2008) 3236.

[2] Tae Jae Lee, Jungeun Seo, Haiwon Lee, Jung Woo Lee and Whikun Yi, “Fabrication of single-walled carbon nanotube three-dimensional networks inside the pores of a porous silicon structure” Carbon, ***(accepted)***

[3] Hyunsook Kim, Tae Jae Lee, Somin Kim and Haiwon Lee, “Modification of silicon substrate using low-energy proton beam for selective growth of CNTs”, J. Nanosci. Nanotech., ***(in final revision)***

2. Conference Presentations

[1] Jeongeun Seo, Tae Jae Lee, Haiwon Lee, “Growth of patterned carbon nanotubes on substrate with functional group by micro contact printing”, NANO KOREA Symposium, KINTEX, Korea, August, 2009.

[2] Taejae Lee, Jungeun Seo, Haegu Yeo, Haiwon Lee, “Synthesis of Single-Walled Carbon Nanotubes on Substrate using Fe-Mo Bimetallic Catalyst”, International Workshop on Nanotechnology and Advanced Functional Materials, PS-92, NCL, Pune, India, Jul 2009.

[3] Jungeun Seo, Tae Jae Lee, Haiwon Lee, Jung Woo Lee, Whikun Yi, “Direct fabrication of single-walled carbon nanotube networks inside pores of three-dimensional porous silicon structures”, Asian Research Network Symposium 2009, P-8, Seoul, Korea, May 2009.

[4] Hyunsook Kim, Tae Jae Lee, Haiwon Lee, “Selective Growing of CNTs on Silicon Substrate Modified by Low-Energy Proton Beam”, Asian Research Network Symposium 2009, P-7, Seoul, Korea, May 2009.

[5] T. J. Lee, J. Seo, S. K. Kim, H. Lee, P. S. Weiss, “Vertical Alignment and Three-Dimensional Networks of Single-Walled Carbon Nanotubes”, 2009 NSTI Nanotechnology Conference and Expo, Houston, TX, May 2009.

[6] T. J. Lee, J. Seo, S. -K. Kim, S. -Kyu Lee, H. Lee, “Diameter Control and Vertical Growth of SWCNTs and Its Potential Applications”, MACRO 2009 – Recent Advances in Polymeric Materials, IIT Madras, INDIA, March 2009 (Invited talk).

[7] T. J. Lee, J. Seo, H. Lee, J. W. Lee, S. Kim, W. Yi, S. K. Kim, S. –H. Han, “Three-Dimensional Networking of Single-Walled Carbon Nanotubes”, 2008 Asian Conference on Nanoscience and Nanotechnology, Singapore, November 2008 (Invited talk).

[8] T. J. Lee, S. K. Kim, J. Seo, S. K. Lee, H. Lee, “Vertical alignment and three-dimensional networking of single-walled carbon nanotubes”, Special Symposium on Emerging Science and Technology, Hanyang University, Korea, June 2008.

[9] T. J. Lee, J. Seo, H. Lee, "Synthesis of directly-connected three-dimensional SWCNT networks in deep holes for applications in future electronics", US-Korea Conference on Science, Technology, and Entrepreneurship, NST-4.3, San Diego, CA, August 2008.

[10] J. E. Seo, T. J. Lee, K. W. Oh, M. M. Sung, J. W. Lee, W. Yi, H. Lee, "Selective growth of CNTs on a patterned substrate with functional group by micro contact printing and their field emission properties", 19th IC ME&D, 2008.

[11] T. J. Lee, J. Seo, J. W. Lee, S. Min, D. S. So, H. Lee, W. Yi, J. W. Lee, S. –H. Han, and H. Lee, “Synthesis and Application of High-Density Single-Walled Carbon Nanotube Networks on Three-Dimensional Si Structures”, The Fall Meeting of Korean Chemical Society,, 금31D9구, 2008. 10.

[11] T. J. Lee, J. Seo, H. Lee, J. W. Lee, and W. Yi, “Direct fabrication of single-walled carbon nanotube networks inside pores of three-dimensional porous silicon structures”, The Spring Meeting of Korean Chemical Society, II32P155포, 2009. 4.

Journal of the Korean Physical Society, Vol. 53, No. 6, December 2008, pp. 3236∼3240

Vertically Aligned Growth of Single-Walled Carbon Nanotubes on an Fe-Mo/MgO/Si Substrate Prepared by Using a Dipping Method Combined with an UV-Ozone Treatment

Tae Jae Lee
Institute of Nano Science and Technology, Hanyang University, Seoul 133-791

Jeongeun Seo
Department of Chemistry, Hanyang University, Seoul 133-791

Haiwon Lee*
Institute of Nano Science and Technology, Hanyang University, Seoul 133-791 and Department of Chemistry, Hanyang University, Seoul 133-791

(Received 7 April 2008, in final form 4 September 2008)

Single-walled carbon nanotubes (SWCNTs) having high density were synthesized on both Fe-Mo/Si and Fe-Mo/MgO/Si substrates by using thermal decomposition of C_2H_2 at 800 °C. By applying an ultraviolet-irradiated-ozone (UV-ozone) treatment to the substrate, high-density catalyst nanoparticles could be attached to not only a Si substrate but also a MgO/Si substrate by using a dipping method. The vertically aligned SWCNTs were successfully synthesized on a MgO/Si substrate after NH_3 pretreatment. Scanning electron microscopy, transmission electron microscopy and Raman spectroscopy were used to characterize the catalyst and the SWCNTs.

PACS numbers: 61.48.+c
Keywords: UV-ozone, Single-walled carbon nanotubes, Chemical vapor deposition, Synthesis

I. INTRODUCTION

Vertically aligned growth of single-walled carbon nanotubes (SWCNTs) on a substrate [1, 2] has attracted much attention due to their potential advantages in several applications, including electronic devices [3], field electron emitters [4–6], solar cells [7] and biosensors [8, 9]. To synthesize SWCNTs on a substrate, various catalyst formation techniques have been investigated [10–16]. Among them, a dipping method has become important because of its simplicity, low-price and easily scaled-up processing. However, SWCNTs synthesized on a substrate prepared by using a dipping method were not vertically aligned; instead, they were laid down with low density [11,17,18]. Murakami *et al.* reported the growth of vertically aligned SWCNTs on a Co-Mo/quartz substrate by drawing up the substrate from a Co-Mo catalyst solution at constant speed [19]. Although their work was successful, the growth of vertically aligned SWCNTs on a substrate prepared by using a dipping method is still a challenge.

Here, we report an efficient formation of Fe-Mo bimetallic nanoparticles on both Si and MgO/Si substrates by using a dipping method combined with an ultraviolet-irradiated-ozone (UV-ozone) treatment of both substrates. Piranha treatment of substrate is reported to be essential to cleaning and modifying the surface of a substrate with a hydroxyl group, which is important catalyst nanoparticles with high density are to be adsorbed onto the substrate when using a dipping method [20]. However, the MgO film was easily damaged and removed from the Si substrate by the piranha treatment. Thus, we could not apply the piranha treatment to clean and modify the MgO/Si substrate. To solve this problem, we applied an UV-ozone treatment instead of the piranha treatment. The UV-ozone treatment not only removed organic contaminants, but also changed the surface properties due to chemical reactions at the surface layers [21–23]. We expected the UV-ozone treatment to clean and modify the surfaces of both Si and MgO/Si substrates.

II. EXPERIMENTS

A p-type Si (p-Si) substrate was cleaned by using ultrasonication with acetone, ethanol and deionized water and was then dried by blowing N_2 on the substrate prior

*E-mail: haiwon@hanyang.ac.kr; Fax: +82-2-2296-0287

to use. A MgO buffer film was deposited on the p-Si substrate by RF magnetron sputtering with ambient Ar at 1.0×10^{-2} Torr. The RF power was 325 W and the deposition rate of the MgO film was 0.2 Å/s. Both the Si and the MgO/Si substrates were treated with UV-ozone by using a commercial UV-ozone cleaner (NL-UV253, G4TS germicidal lamp using a wavelength of 253.7 nm, produced by Nippon Laser & Electronics Lab) for 2 h.

A Fe-Mo bimetallic catalyst solution was prepared using ethanol. The concentrations of Fe and Mo in the catalyst solution were both 0.01 M. Briefly, 202 mg of $Fe(NO_3)_3{\cdot}9H_2O$ (assay min. 98.0 %, Junsei) and 4.895 ml of Mo solution (ICP/DCP standard solution, 10,000 μg/mL Mo in H_2O, Aldrich) were dissolved in 50 ml of ethanol (assay min. 99.9 %, Fisher) with ultrasonication for 30 min. In order to attach the Fe-Mo bimetallic catalyst onto both the Si and the MgO/Si substrates, we soaked the UV-ozone-treated substrates in the catalyst solution for 10 min at room temperature and then thoroughly rinsed them with ethanol. After that, the substrates were treated with UV-ozone [24] for 10 h by using the same UV-ozone cleaner as used above.

The growth of carbon nanotubes (CNTs) was carried out in a horizontal quartz tube reactor. The catalyst-adsorbed substrates were inserted into the center of the quartz tube reactor. Subsequently, the reactor was pumped down to less than 1.0×10^{-2} Torr and heated up to 800 °C. When the temperature of reactor had reached 800 °C, the NH_3 pretreatment was performed to reduce the metal oxide to the metal catalyst [13] by introducing 500 sccm of NH_3 gas into the reactor for 10 min. Also, 20 sccm of C_2H_2 was introduced for 10 min to grow the CNTs so that the pressure inside the reactor was maintained at 3.3×10^{-1} Torr. After that, the reactor was pumped down to less than 1.0×10^{-2} Torr and cooled down to room temperature.

The substrates and the CNTs were characterized by using scanning electron microscopy (SEM, S-4700, Hitachi) and transmission electron microscopy (TEM, TECNAI-F20, 200 keV, Philips; TECNAI-F30 S-Twin, 300 keV, Philips). For the TEM analysis, CNTs were first dispersed in an ethanol solvent by ultrasonication for 2 h. The CNTs solution was then dropped on the TEM grid (carbon-coated micro-pore Cu grid, 200 mesh) several times using a micropipette and dried in ambient air at room temperature. Raman spectroscopy (LabRam HR, 514-nm laser excitation wavelength, Jobin-Yvon; NRS-3000, 532-nm laser excitation wavelength, Jasco; Nanofinder-30, 488-nm and 633-nm laser excitation wavelengths, Tokyo Instruments Co.) was used to investigate the diameter distribution of the SWCNTs.

III. RESULTS ANS DISCUSSION

Figure 1(a) shows that the Fe-Mo nanoparticles were successfully formed with a high density on the UV-ozone-treated Si substrate by using the dipping method because the surface of the Si substrate was fully cleaned and hydroxylated by the UV-ozone treatment [23], which is important for efficient nanoparticle formation from the ionic catalyst solution [11, 20]. The yield of SWCNTs grown on the Fe-Mo/Si substrate was, however, quite low as shown in Figure 1(b). When the NH_3 pretreatment was applied, the yield of SWCNTs greatly increased due to the catalyst activation [13], but the SWCNTs still lay on the substrate (Figure 1(c)) because the density of the active Fe-Mo catalyst nanoparticles was decreased by iron sintering into the Si substrate and forming metal silicide [26, 27]. To avoid the iron sintering into the Si substrate, we deposited MgO buffer films onto the Si substrates. The MgO has been successfully adopted for the massive synthesis of SWCNTs as a supporting material [24]. Moreover, the SWCNTs synthesized on the

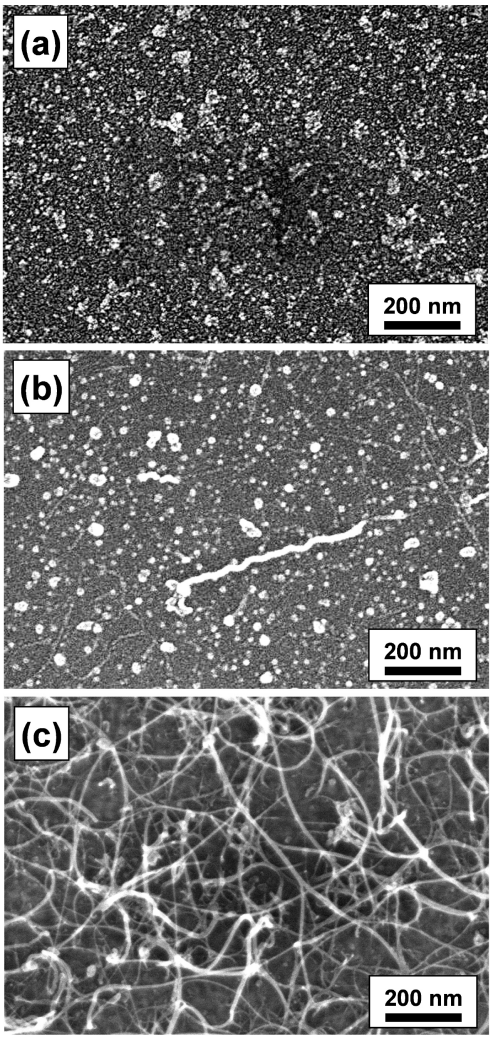

Fig. 1. (a) SEM image of Fe-Mo catalyst nanoparticles adsorbed on a Si substrate by using a dipping method. SEM images of SWCNTs grown on an Fe-Mo/Si substrate (b) without NH_3 pretreatment and (c) with NH_3 pretreatment.

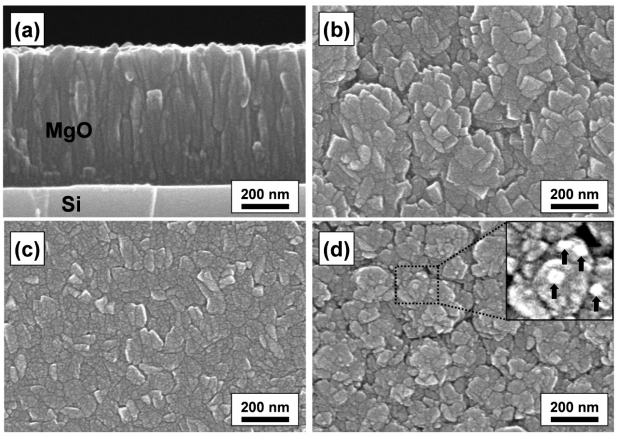

Fig. 2. SEM images of (a) a side view of a pristine MgO film, (b) a top view of a pristine MgO film, (c) a top view of an Fe-Mo-adsorbed MgO film and (d) a top view of an Fe-Mo/MgO film annealed at 800 °C for 10 min in vacuum. The inset in Figure 2(d) is the enlarged SEM image of the Fe-Mo nanoparticles, indicated with black arrows.

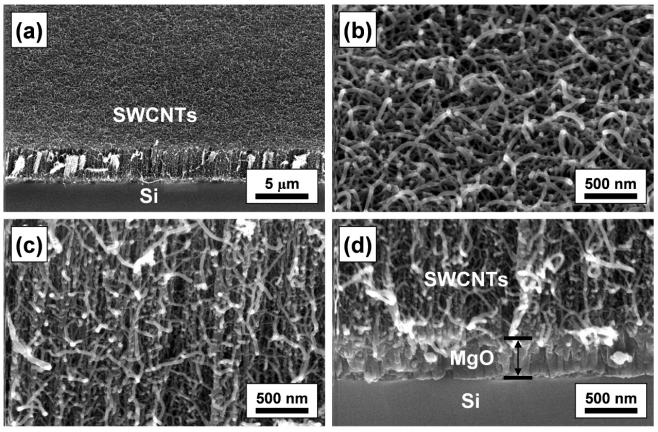

Fig. 3. SEM images of vertically aligned SWCNTs grown on an Fe-Mo/MgO/Si substrate; (a) cut edge, (b) top surface, (c) middle side and (d) bottom side.

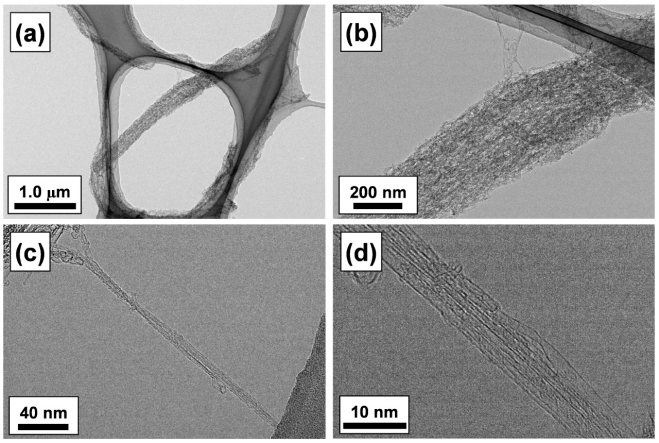

Fig. 4. TEM images of vertically aligned SWCNTs grown on an Fe-Mo/MgO/Si substrate; (a) and (b) low magnification images of SWCNT super bundles and (c) and (d) high magnification images of one SWCNT bundle.

MgO films can be used for the GaN-based electronic devices as a gate electrode/gate oxide [28,29].

Figure 2(a) shows that the MgO buffer films (thickness is about 550 nm) were uniformly deposited on the Si substrates. The surfaces of MgO buffer films were rough, with many grains of various sizes (Figure 2(b)). The UV-ozone-treated MgO buffer films were also revealed to have the same surface morphologies as the as-deposited one. By adsorbing the Fe-Mo catalyst species through the dipping method, the surfaces of the MgO buffer films were changed, as shown in Figure 2(c). Figure 2(d) showed that the Fe-Mo bimetallic nanoparticles (sized below 40 nm) appeared on the surface of the MgO buffer films after the Fe-Mo/MgO/Si substrate had been heated from the room temperature to the SWCNTs growth temperature (800 °C). The density of the Fe-Mo catalyst nanoparticles formed on the MgO/Si substrate was similar to that of the Fe-Mo formed on the Si substrate (Figure 1(a)).

SEM analysis of the SWCNTs revealed that vertical SWCNTs were uniformly grown over the whole area of the Fe-Mo/MgO/Si substrate (Figure 3(a)). This vertical growth of SWCNTs occurred because the high-density catalyst nanoparticles had been fully activated by using MgO buffer films to suppress the iron sintering into the Si substrate [24]. The vertical length of the SWCNTs was about 5 μm and all the SWCNTs had a noodle shapes with clean surfaces (Figures 3(b) and 3(c)). The roots of the SWCNTs have strong binding with the MgO buffer films (Figure 3(d)).

TEM images (Figure 4) showed that the vertically aligned SWCNTs had a bundle structure. Thus, the diameters of the SWCNT bundles were smaller than 40 nm, as shown in Figures 3(b)-(d). The TEM images (Figure 4(d)) also showed that the SWCNTs had clean surfaces without carbon impurities and that the crystallinity of the SWCNTs was good.

Raman analysis [30,31] was performed to investigate both the diameter distributions and the crystallinity of the SWCNTs (Figure 5). The diameter of the SWCNTs was calculated by using $d^{0.93}$ (nm) $= 238/v_{RBM}$ (cm^{-1}), where v_{RBM} is the radial breathing mode (RBM) frequency and d is the diameter of the SWCNTs. The assignments of metallic (**M**) SWCNTs are indexed in Figure 5(b) based on the Kataura plot [32]. Figures 5(a(1)) and 5(b(1)) show clear RBMs at about $100 - 300$ cm^{-1}, a strong D-band at $1306 - 1335$ cm^{-1} and a sharp G-band at $1571 - 1592$ cm^{-1}. The Raman spectra reveal that the SWCNTs have wide diameter distributions corresponding to various electrical properties. The strong D-bands imply that a small number of amorphous carbon impurities or structural defects of the graphite walls exist in the SWCNT bundles.

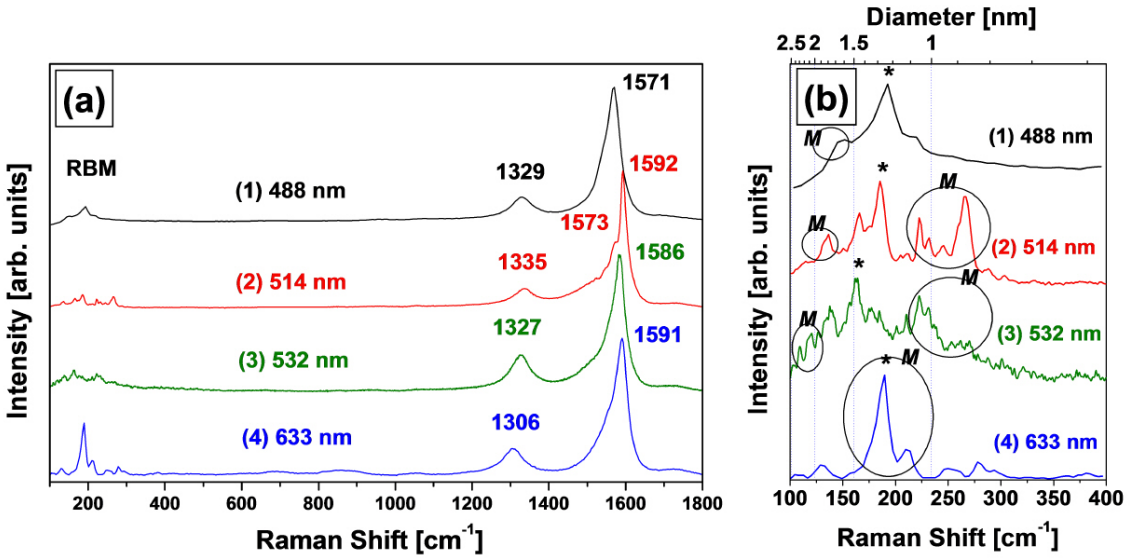

Fig. 5. Raman spectra of vertically aligned SWCNTs grown on an Fe-Mo/MgO/Si substrate. (a) Whole frequency range from the RBM to the G band. (b) Enlarged view of the RBM frequency range. The spectra in (a) are normalized to each G-band at 1571 – 1592 cm^{-1} and the spectra in (b) are normalized to the highest peaks marked with an asterisk (∗). The wavelengths of the excitation lasers are 488 nm (1), 514 nm (2), 532 nm (3) and 633 nm (4).

IV. CONCLUSION

In conclusion, we synthesized high-density SWCNTs on both Fe-Mo/Si and Fe-Mo/MgO/Si substrates prepared by using a dipping method. The UV-ozone treatment was useful to attach high-density catalyst nanoparticles uniformly onto both the Si and the MgO/Si substrates. As a result, vertically aligned SWCNTs (vertical length was 5 μm) were successfully synthesized on the Fe-Mo/MgO/Si substrate. SEM, TEM and Raman analyses revealed that the vertically aligned SWCNTs had a bundle structure with clean surfaces and good crystallinity. However, the strong D-bands in Raman spectra imply that a small number of amorphous carbon impurities or structural defects in the graphite walls existed in the SWCNT bundles. This result will be useful in forming high-density metal nanoparticles on various substrates by using a dipping method and for the synthesis of vertically aligned SWCNTs at low cost.

ACKNOWLEDGMENTS

The authors thank Professor Whikun Yi and Mr. Jung Woo Lee for providing the MgO buffer films. This work was supported by a grant (08K1501-02011) from 'Center for Nanostructured Materials Technology' under '21st Century R&D Programs' of the Ministry of Education, Science and Technology, Korea and by a grant (AOARD-08-4004) from AFOSR/AOARD, U.S.A.

REFERENCES

[1] K. Hata, D. N. Futaba, K. Mizuno, T. Namai, M. Yumura and S. Iijima, Science **306**, 1362 (2004).
[2] G. Zhang, D. Mann, L. Zhang, A. Javey, Y. Li, E. Yenilmez, Q. Wang, J. P. McVittie, Y. Nishi, J. Gibbons and H. Dai, Proc. Natl. Acad. Sci. U.S.A. **102**, 16141 (2005).
[3] A. P. Graham, G. S. Duesberg, R. V. Seidel, M. Liebau, E. Unger, W. Pamler, F. Kreupl and W. Hoenlein, Small **1**, 382 (2005).
[4] N. S. Lee, D. S. Chung, I. T. Han, J. H. Kang, Y. S. Choi, H. Y. Kim, S. H. Park, Y. W. Jin, W. K. Yi, M. J. Yun, J. E. Jung, C. J. Lee, J. H. You, S. H. Jo, C. G. Lee and J. M. Kim, Diam. Relat. Mater. **10**, 265 (2001).
[5] K. S. Park, H. S. Yoon, J. H. Ryu, S. H. Lim, J. H. Moon and J. Jang, J. Korean Phys. Soc. **48**, 1365 (2006).
[6] C.-D. Kim, Y.-J. Kim, H.-W. Ryu, J.-T. Kang, S. Kim, B.-K. Min and H.-R. Lee, J. Korean Phys. Soc. **51**, 193 (2007).
[7] J. Rud, L. Lovell, J. Senn, Q. Qiao and J. McLeskey, J. Mater. Sci. **40**, 1455 (2005).
[8] J. Li, H. T. Ng, A. Cassell, W. Fan, H. Chen, Q. Ye, J. Koehne, J. Han and M. Meyyappan, Nano Lett. **3**, 597 (2003).
[9] Y. Lin, F. Lu, Y. Tu and Z. Ren, Nano Lett. **4**, 191 (2004).
[10] J. Kong, H. T. Soh, A. M. Cassell, C. F. Quate and H. Dai, Nature **395**, 878 (1998).
[11] H. C. Choi, S. Kundaria, D. Wang, A. Javey, Q. Wang, M. Rolandi and H. Dai, Nano Lett. **3**, 157 (2003).
[12] S. Han, T. Yu, J. Park, B. Koo, J. Joo, T. Hyeon, S. Hong and J. Im, J. Phys. Chem. B **108**, 8091 (2004).
[13] M. Cantoro, S. Hofmann, S. Pisana, V. Scardaci, A. Parvez, C. Ducati, A. C. Ferrari, A. M. Blackburn, K.

Y. Wang and J. Robertson, Nano Lett. **6**, 1107 (2006).
[14] B. S. Oh, Y.-S. Min, E. J. Bae, D. Kang, I. S. Jung, C. S. Hwang, Y. K. Kim and W. Park, J. Mater. Chem. **16**, 174 (2006).
[15] T. Iwasaki, R. Morikane, T. Edura, M. Tokuda, K. Tsutsui, Y. Wada and H. Kawarada, Carbon **45**, 2351 (2007).
[16] Y. Yao, Q. Li, J. Zhang, R. Liu, L. Jiao, Y. T. Zhu and Z. Liu, Nat. Mater. **6**, 283 (2007).
[17] Y. Murakami, Y. Miyauchi, S. Chiashi and S. Maruyama, Chem. Phys. Lett. **377**, 49 (2003).
[18] M. He, X. Ling, J. Zhang and Z. Liu, J. Phys. Chem. B **109**, 10946 (2005).
[19] Y. Murakami, S. Chiashi, Y. Miyauchi, M. Hu, M. Ogura, T. Okubo and S. Maruyama, Chem. Phys. Lett. **385**, 298 (2004).
[20] H. J. Yang, H. J. Song, H. J. Shin and H. C. Choi, Langmuir **21**, 9098 (2005).
[21] R. R. Sowell, R. E. Cuthrell, D. M. Mattox and R. D. Bland, J. Vac. Sci. Technol. **11**, 474 (1974).
[22] M.-P. Chen, K. Kuroishi and Y. Kitamoto, Electrochimica Acta **51**, 860 (2005).
[23] M. Tominaga, N. Hirata and I. Taniguchi, Electrochem. Comm. **7**, 1423 (2005).
[24] T. J. Lee and H. Lee, Carbon **46**, 1443 (2008).
[25] D. Q. Duy, H. S. Kim, D. M. Yoon, J. H. Kim, J. W. Ha, K. J. Lee, Y. G. Hwang, C. H. Lee and B. T. Cong, J. Korean Phys. Soc. **53**, 2568 (2008).
[26] M. Liehr, H. Lefakis, F. K. LeGoues and G. W. Rubloff, Phys. Rev. B **33**, 5517 (1986).
[27] L. Delzeit, B. Chen, A. Cassell, R. Stevens, C. Nguyen and M. Meyyappan, Chem. Phys. Lett. **348**, 368 (2001).
[28] J. Kim, B. Gila, R. Mehandru, J. W. Johnson, J. H. Shin, K. P. Lee, B. Luo, A. Onstine, C. R. Abernathy, S. J. Pearton and F. Ren, J. Electrochem. Soc. **149**, G482 (2002).
[29] Y. Irokawa, Y. Nakano, M. Ishiko, T. Kachi, J. Kim, F. Ren, B. P. Gila, A. H. Onstine, C. R. Abernathy, S. J. Pearton, C.-C. Pan, G.-T. Chen and J.-I, Chyi, Appl. Phys. Lett. **84**, 2919 (2004).
[30] J. L. Sauvajol, E. Anglaret, S. Rols and L. Alvarez, Carbon **40**, 1697 (2002).
[31] M. Burghard, Surf. Sci. Rep. **58**, 1 (2005).
[32] H. Kataura, Y. Kumazawa, Y. Maniwa, I. Umezu, S. Suzuki, Y. Ohtsuka and Y. Achiba, Syn. Met. **103**, 2555 (1999).

View Letter

Close

Date: 2009-12-17 07:36:54
To: "Haiwon Lee" haiwon@hanyang.ac.kr
From: Chong Rae Park crpark@snu.ac.kr
Subject: Your Submission

Ms. Ref. No.: CARBON-D-09-01164R2
Title: Fabrication of single-walled carbon nanotube three-dimensional networks inside the pores of a porous silicon structure
CARBON

Dear haiwon,

I am pleased to confirm that your paper "Fabrication of single-walled carbon nanotube three-dimensional networks inside the pores of a porous silicon structure" has been accepted for publication in CARBON.

Thank you for submitting your work to this journal.

With kind regards,

Chong Rae Park, PhD
Editor
CARBON

Reviewers' comments:

Close

Elsevier Editorial System(tm) for CARBON
Manuscript Draft

Manuscript Number: CARBON-D-09-01164R2

Title: Fabrication of single-walled carbon nanotube three-dimensional networks inside the pores of a porous silicon structure

Article Type: Research Paper

Corresponding Author: Professor Haiwon Lee, Ph. D.

Corresponding Author's Institution: Hanyang University

First Author: Tae Jae Lee, Ph.D.

Order of Authors: Tae Jae Lee, Ph.D.; Jungeun Seo; Haiwon Lee, Ph.D.; Jung Woo Lee, M.D.; Whikun Yi, Ph.D.

Abstract: Single-walled carbon nanotube (SWCNT) three-dimensional (3-D) networks were first fabricated in the pores of a porous silicon substrate using thermal decomposition of C2H2 at 800°C. Catalyst nanoparticles were uniformly distributed on the inner wall surfaces of the pores using a dipping method combined with ultrasonication. SWCNTs were synthesized along the inner wall surface of the pores, and spanned it. The suspended SWCNTs inside the pores formed 3-D networks in the results of the chaotic overgrowth of SWCNTs in a confined space under thermal vibration, and van der Waals interactions between SWCNTs.

Fabrication of single-walled carbon nanotube three-dimensional networks inside the pores of a porous silicon structure

Tae Jae Lee [a], *Jungeun Seo* [b], *Haiwon Lee* [a,b,*], *Jung Woo Lee* [b] *and Whikun Yi* [b]

[a]Institute of Nano Science and Technology, Hanyang University, Seoul 133-791, Korea

[b]Department of Chemistry, Hanyang University, Seoul 133-791, Korea

Abstract

Single-walled carbon nanotube (SWCNT) three-dimensional (3-D) networks were first fabricated in the pores of a porous silicon substrate using thermal decomposition of C_2H_2 at 800°C. Catalyst nanoparticles were uniformly distributed on the inner wall surfaces of the pores using a dipping method combined with ultrasonication. SWCNTs were synthesized along the inner wall surface of the pores, and spanned it. The suspended SWCNTs inside the pores formed 3-D networks in the results of the chaotic overgrowth of SWCNTs in a confined space under thermal vibration, and van der Waals interactions between SWCNTs.

1. Introduction

Suspension of single-walled carbon nanotube (SWCNT) between two electrodes is of interest both academically and practically.[1-6] Several groups have reported the synthesis and potential applications of SWCNTs suspended between two electrodes, especially in the pillar structure.[7-13] These studies focused on the synthesis of individual SWCNT bridges or high-density SWCNT networks as a channel

*Corresponding author. Tel.: +82-2-2220-0945; Fax: +82-2-2296-0287; E-mail address: haiwon@hanyang.ac.kr (Haiwon Lee)

or a connecting wire for nano-sized electronic devices. Simultaneously, it has been also reported that vertically aligned carbon nanotubes (CNTs) were synthesized inside the pores of either a patterned SiO_2 substrate[14] or a porous anodic alumina template[15, 16] by forming a metal catalyst only on the bottom of the pores as shown in Fig 1a-c. However, it has not yet been reported that a suspended bridge or a network of SWCNTs was synthesized inside a tubular structure (Fig. 1f). The network structure of SWCNTs can be used for microfluidic chips[17, 18] as nano-sized filters[19, 20] or sensing channels[21]. Herein, we first report the synthesis of SWCNT 3-D networks inside the pores of a porous silicon substrate with a complex tubular structure (see Fig. S1). To synthesize a SWCNT three-dimensional (3-D) network inside a tubular structures such as a hole or a deep pore, catalyst nanoparticles need to be deposited uniformly on the whole inner wall surface of those tubular structures. A dipping method combined with ultrasonication[22] was utilized to stimulate the formation of catalyst nanoparticles over the entire area of the porous silicon substrate. As a result the SWCNT 3-D networks were uniformly synthesized inside the pores of the porous silicon substrate. Schematics of the fabrication process for the SWCNT 3-D networks are shown in Figs. 1d-f.

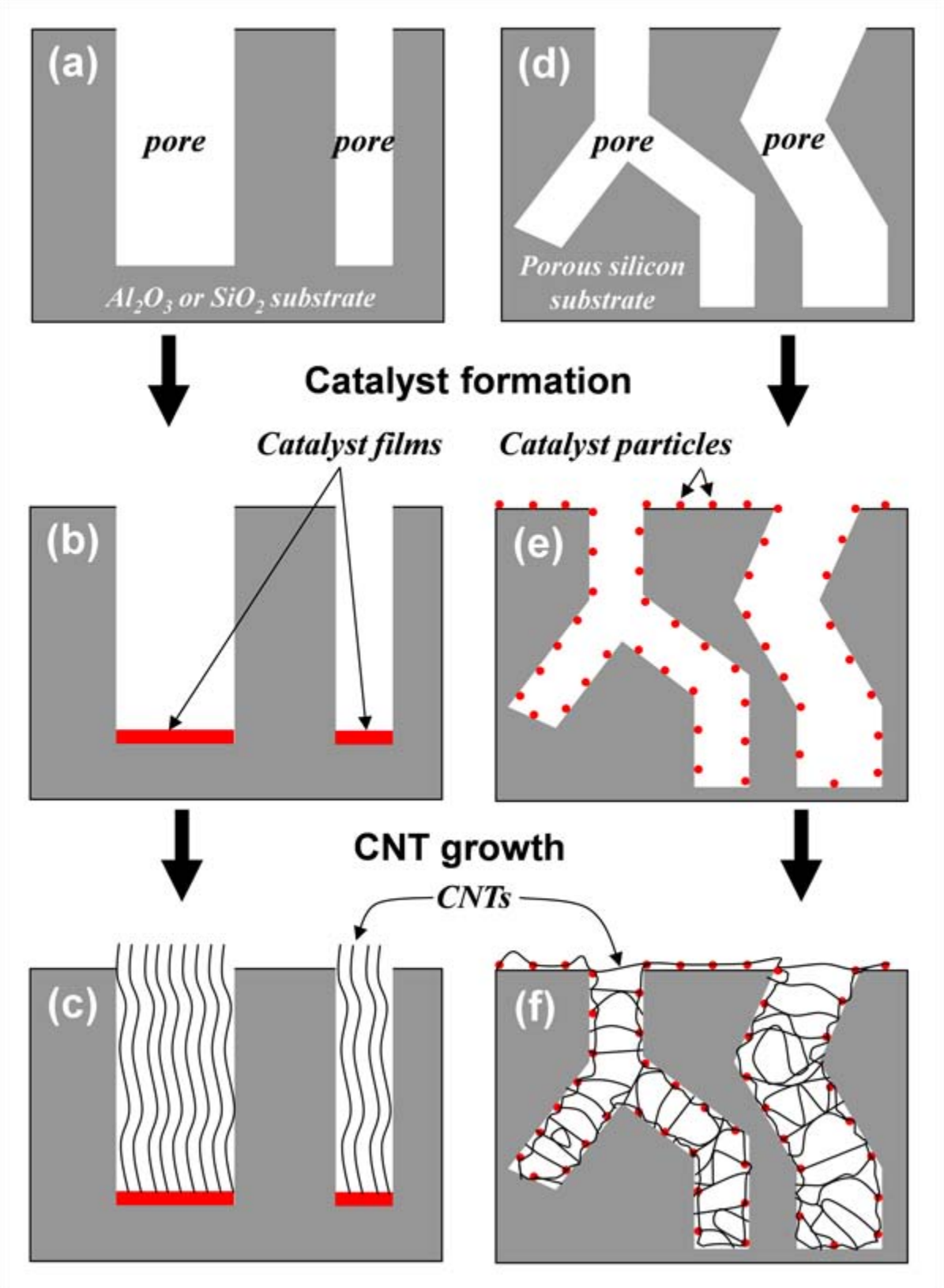

Fig. 1. Schematics of the fabrication processes for synthesizing (a-c) vertically aligned CNTs and (d-f) SWCNT 3-D networks inside the pores of porous structures.

2. Experimental

2.1. *Preparation of the porous silicon substrate*

A porous silicon layer was fabricated on the surface of a silicon wafer using a common electrochemical etching technique.[23] Briefly, an n-type silicon (100) wafer was placed into a mixture of HF and ethanol solvent. Then, a porous silicon layer with complex pores (diameter of 200 – 1,000 nm and depth of ~ 40 μm) was formed (Figs. 2a-c) by applying a DC voltage with a white light (white halogen lamp; 50 W) for 40 min. The porous silicon substrate was cleaned by ultrasonication in acetone, ethanol, and deionized water (DI water) sequentially. The as-prepared porous silicon substrate was cleaned and modified with hydroxyl group by socking it into Piranha solution (H_2SO_4:H_2O_2=3:1) for 30 min.[24] The porous silicon substrate was then washed by ultrasonication in DI water to remove the piranha solution from the pores. The surface morphologies of both the top and inner surface of the pores were very rough (Figs. 2c and d).

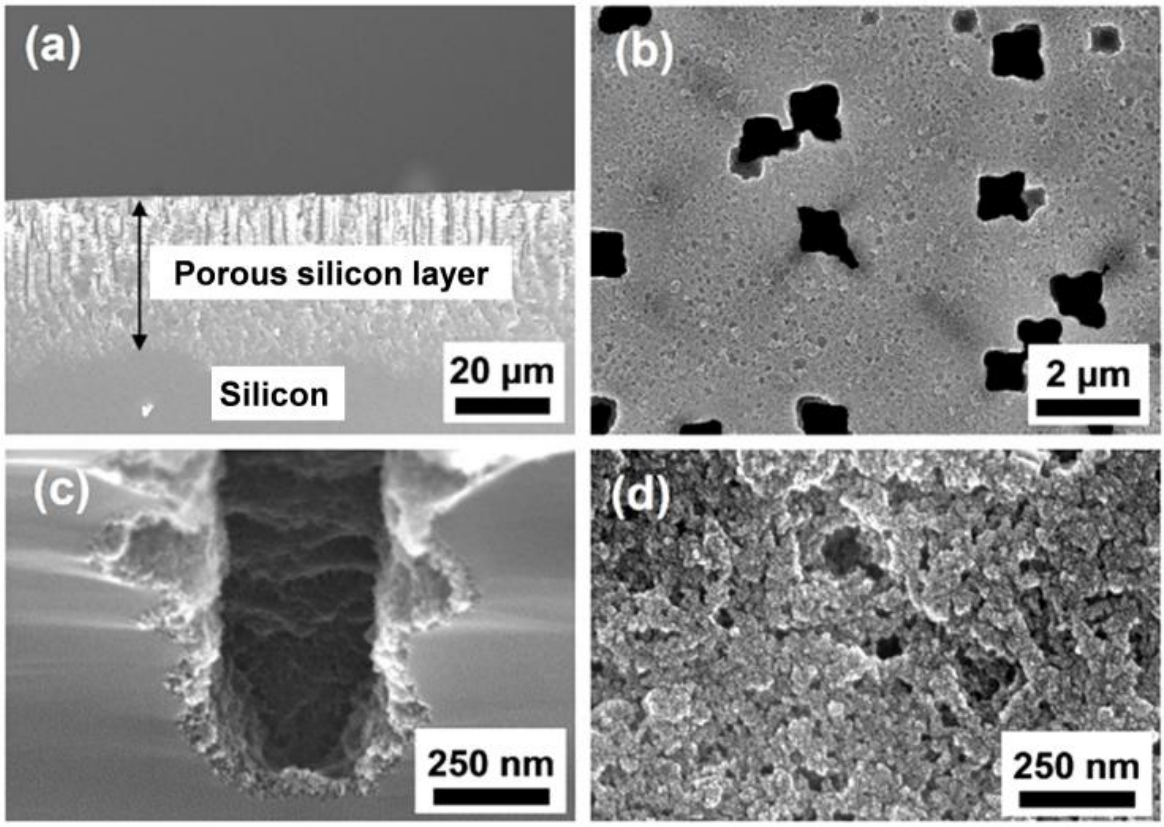

Fig. 2. SEM images of the pristine porous silicon substrate: (a) Cut edge, (b) Top surface, (c) Bottom of a pore, and (d) Enlarged top surface.

2.2. *Catalyst formation by a dipping method*

An Fe-Mo bimetallic catalyst solution [25] was prepared by ultrasonication using an ethanol solvent, $Fe(NO_3)_3 \bullet 9H_2O$ (Junsei), and a Mo solution (ICP/DCP standard solution, Aldrich). The molar ratio of Fe/Mo in the catalyst solution was 4/1. To deposit the Fe-Mo bimetallic catalyst on the inner wall surface of the pores of the porous silicon substrate, the substrate was soaked in the Fe-Mo catalyst solution for 20 minutes with ultrasonication, and then washed thoroughly in ethanol solvent several times. Catalyst solution was dispersed uniformly on the whole area of porous silicon substrate including the bottom of deep pores by applying an ultrasonication during the dipping process. The density of catalyst nanoparticle was controlled by adjusting the concentration of "Fe" in ethanol solvent. The concentration of "Fe" was 10 mM.

2.3. *Synthesis of SWCNTs*

SWCNTs were synthesized in a horizontal quartz tube reactor. The diameter and the length of the reactor are 40 and 800 mm, respectively. The catalyst-formed porous silicon substrate was annealed at 400°C for 30 min in ambient air. Subsequently, the reactor was pumped down to 9.0×10^{-3} torr and heated to 800°C. When the temperature of the reactor reached 800°C, 300 sccm of NH_3 gas was introduced into the reactor for 10 min to reduce the iron oxide to the iron catalyst.[26] After the NH_3 pretreatment, 10 sccm of C_2H_2 gas was introduced for 10 min to synthesize SWCNTs while maintaining a pressure of 3.3×10^{-1} torr. Finally, the reactor was cooled down to room temperature under a pressure of 9.0×10^{-3} torr.

2.4. *Characterization of catalyst deposition and SWCNTs*

Atomic force microscopy (AFM: Nanoscope 3a, Digital Instruments) was used to image the catalyst nanoparticles that formed on the silicon surfaces. Scanning electron microscopy (SEM: S-4800, Hitachi), transmission electron microscopy (TEM: TECNAI-F20, 200 keV, Philips), and Raman spectroscopy (LabRam HR, 514 nm laser excitation wavelength, Jobin-Yvon) were used to characterize the morphology, structure, and crystallinity of the as-synthesized SWCNTs.

3. Results and Discussion

The rough surface morphology of the pristine porous silicon substrate (Fig. 2d) prevented us from imaging catalyst nanoparticles formed either on the inner wall surface of the pores or on the top surface of the porous silicon substrate. To evaluate the formation of catalyst nanoparticles on the silicon surface, we therefore deposited the catalyst nanoparticles on a planar silicon substrate instead of on the porous silicon substrate using the same dipping conditions. The catalyst nanoparticles deposited on a planar silicon substrate by the dipping method are shown in Fig. 3. The roughness and the average particle

height of the catalysts were 1.8 and 7.6 nm, respectively. It should be noted that the inner wall surface of the pores is different from that of planar silicon, therefore the population of catalyst nanoparticles would differ between these two different substrates. Nevertheless, SEM images of SWCNTs shown in Fig.4 imply that the catalyst nanoparticles were also formed both on the top surface and inside the pores of a porous silicon substrate.

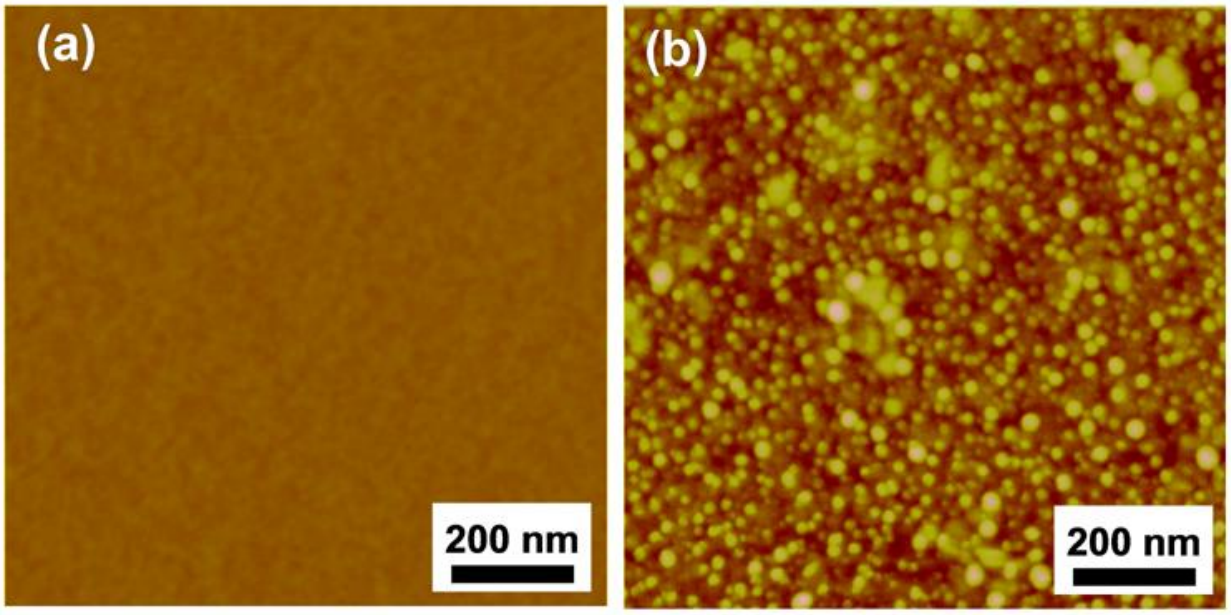

Fig. 3. AFM images of (a) a planar silicon substrate, and (b) catalyst nanoparticles formed on a planar silicon substrate by dipping method.

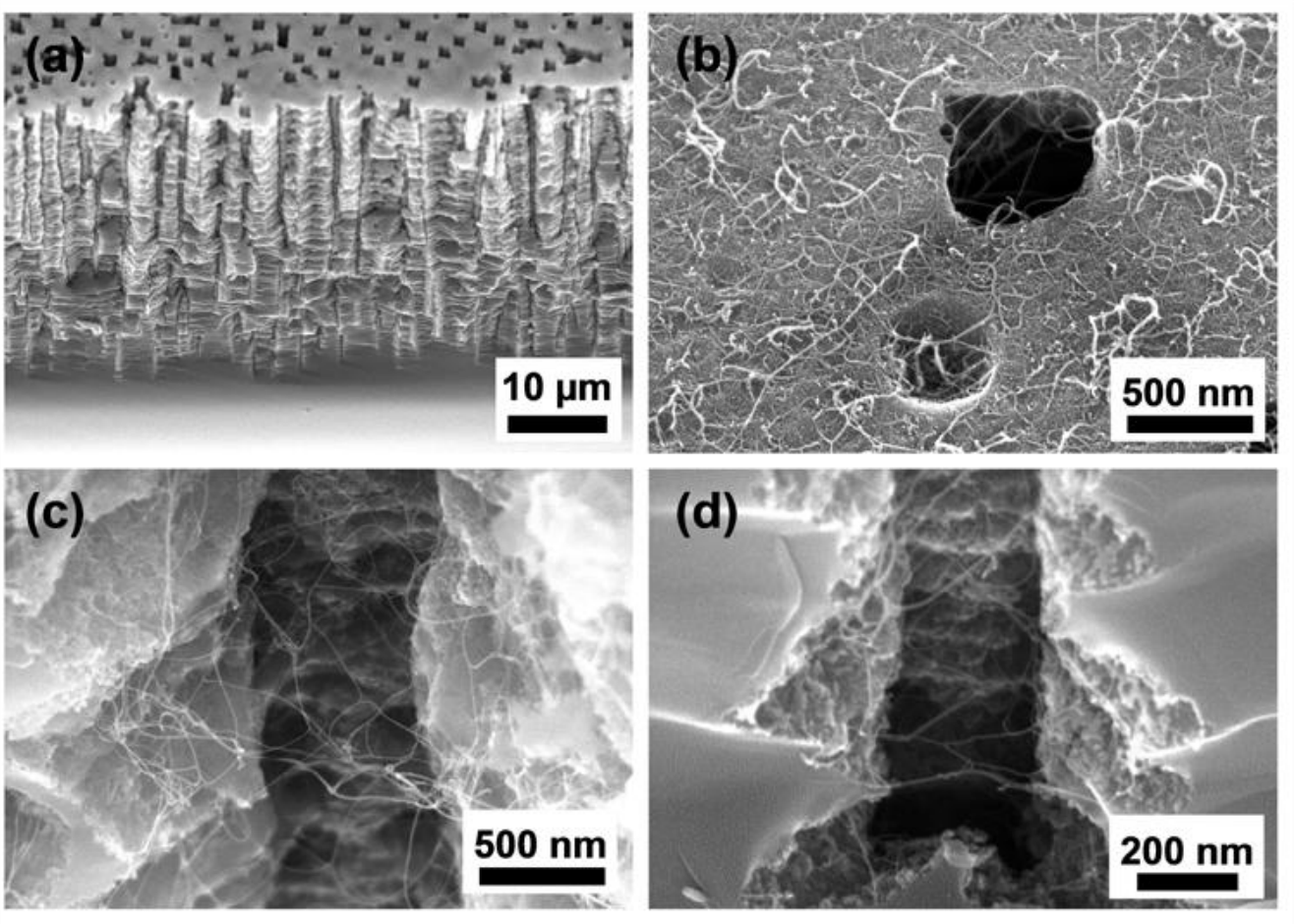

Fig. 4. SEM images of SWCNTs synthesized on a porous silicon substrate: (a) Cut edge under low magnification, (b) Top surface, (c) Middle area of a pore, and (d) Bottom area of a pore.

SEM images of the as-synthesized SWCNTs formed on a porous silicon substrate by thermal decomposition of C_2H_2 at 800°C for 10 min are shown in Fig. 4. Most SWCNTs synthesized on the top surface had a noodle-like shape and formed two-dimensional network along the top surface (Fig. 4b). The SWCNTs inside the pores were not only synthesized along the inner wall surfaces of the pores but also spanned it with various shapes and directions, resulting in the SWCNT 3-D networks (Figs. 4c-d, S1b, and S2). SEM analysis also revealed that the SWCNT 3-D networks were formed throughout the pores without multi-walled carbon nanotubes. This implies that uniform catalyst nanoparticles were deposited throughout the inner wall surface of the pores by the dipping method.

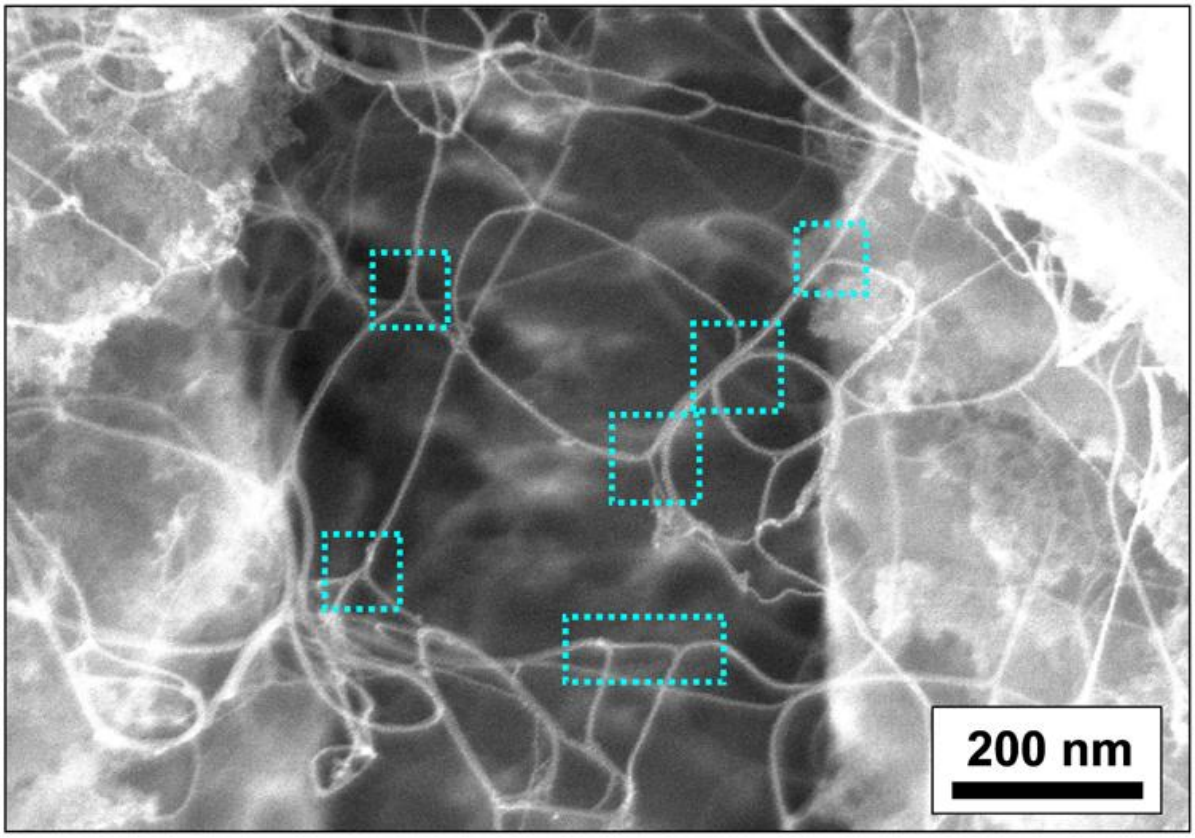

Fig. 5. Magnified SEM image of the SWCNT 3-D networks synthesized in the pore of a porous silicon substrate. The squares drawn with a dotted line indicate the joints of the SWCNT networks.

Figure 5 shows that the SWCNTs made "**Y**"-shaped contacts in 3-D space, forming a SWCNT 3-D network. It is likely that the SWCNT 3-D network is the outcome of both the simple chaotic overgrowth of SWCNTs in a confined space under thermal vibration, [27, 28] and van der Waals interactions between the SWCNTs. [29] It should be noted that we could not directly estimate the diameter of either an individual SWCNT or a bundle of SWCNTs in SEM images because a single-line of CNT shown in SEM image (i.e. Fig 5) can be either a single SWCNT or a bundle of SWCNTs as shown in Fig. 6.

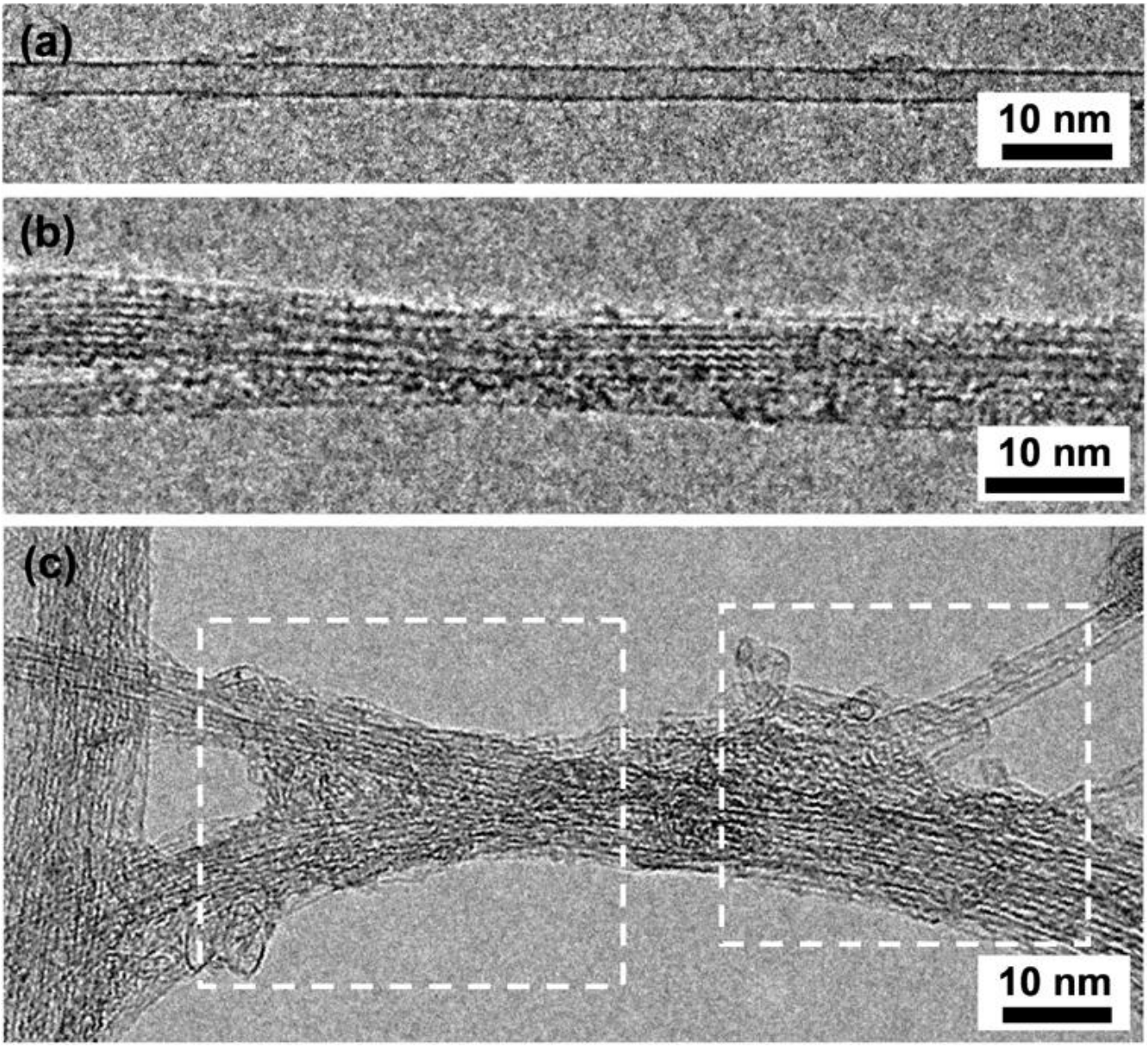

Fig. 6. TEM images of (a) an individual SWCNT, (b) a bundle of SWCNTs, and (c) a SWCNT network synthesized in the pores of a porous silicon substrate. The squares drawn with a dotted line indicate the joints of the SWCNT network.

TEM analysis revealed that the as-synthesized SWCNTs are either an individual SWCNT or a bundle of SWCNTs with various diameters (Figs. 6a-b). The SWCNTs have a clean surface, and good crystallinity. Figure 6c clearly shows that the "**Y**"-shaped contacts of the SWCNT 3-D network were made up by van der Waals interactions between SWCNTs.[28, 29]

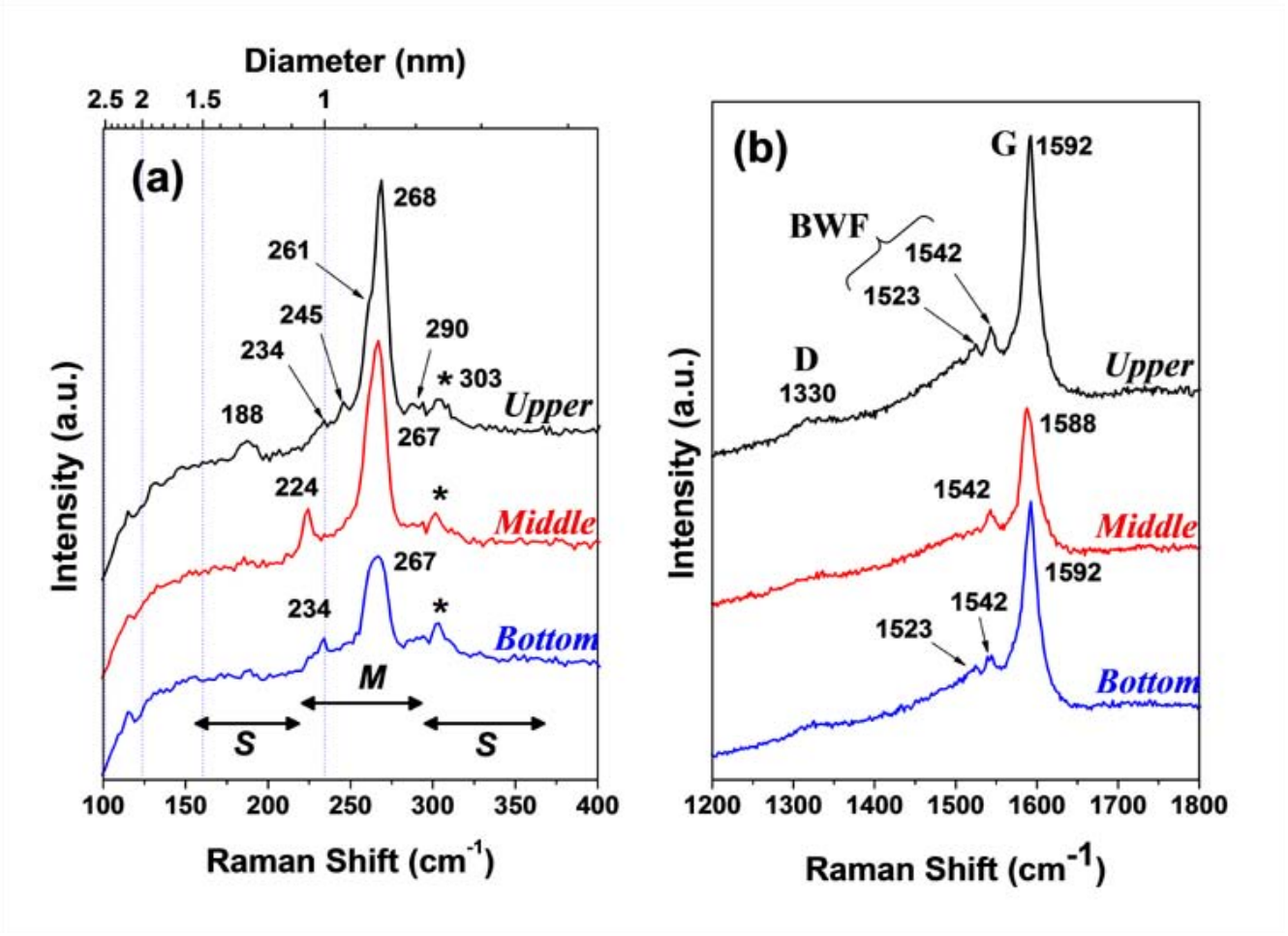

Fig. 7. Raman spectra of the SWCNT 3-D networks synthesized in different areas (such as upper, middle, and bottom areas) of a pore: (a) RBM frequency range, and (b) G and D frequency range. The wavelength of the excitation laser was 514 nm.

Raman spectra of the SWCNT 3-D networks synthesized in different areas of a pore are shown in Fig. 7. The diameter of SWCNTs was calculated by applying the formula, $d^{0.93}$ (nm) = 238/ν_{RBM} (cm^{-1}), where ν_{RBM} is the radial breathing mode (RBM) frequency and d is the diameter of the SWCNT.[30, 31] The assignments of metallic (***M***) and semi-conducting (***S***) SWCNTs indexed in Fig. 7a are based on a Kataura plot.[32] Clear RBMs at 100-300 cm^{-1}, a weak D-band at 1,330 cm^{-1}, clear Breit-Wigner-Fano (BWF)- bands[32] at 1,523-1,542 cm^{-1}, and a sharp G-band at 1,588-1,592 cm^{-1} are evident in the Raman spectra. These findings imply that the SWCNTs were synthesized throughout the pores. The

weak intensity of the D-bands indicates that the SWCNTs had good crystallinity. The shapes of the RBMs (Fig. 7a) indicate that metallic SWCNTs with small diameters (about 0.8-1.1 nm) were synthesized inside the pores. Consistent with this, BWF peaks at 1,523 and 1,542 cm^{-1}, corresponding to metallic SWCNTs, were clearly visible (Fig. 7b). Although the Raman spectra of SWCNTs show a single strong peak in RBM frequency range throughout the pore, it is not directly indicating that most SWCNTs have uniform diameter of 0.87 nm (corresponding at 268 cm^{-1}) as revealed in TEM analysis (Fug. 6).

4. Conclusions

The SWCNT 3-D networks were first fabricated inside the pores of a porous silicon substrate by thermal decomposition of C_2H_2 at 800°C. A dipping method combined with ultrasonication was good for the formation of uniform catalyst nanoparticles on the inner wall surface throughout the pores. The SWCNTs inside the pores were not only synthesized along the inner wall surfaces of the pores but also spanned it with various shapes and directions, resulting in the SWCNT 3-D networks. SEM, TEM, and Raman analysis showed that the SWCNTs have a clean surface and a good crystallinity. It was also revealed that the SWCNT 3-D networks were made up by bundling between SWCNTs. Our findings will inform the fabrication of nano-sized filters or sensing channels for application in future microfluidic chips.

Acknowledgments

We would like to thank Miss Hyunsook Kim for her help with AFM measurements. This work was supported by a grant (08K1501-02011) from the ‘Center for Nanostructured Materials Technology’ under the ‘21st Century Frontier R&D Programs’ of the Ministry of Education, Science and Technology (MEST) of Korea, by a grant (AOARD-08-4004) from AFOSR/AOARD of USA, and also by the International Research & Development Program of the National Research Foundation of Korea

(NRF) funded by the MEST of Korea (Grant number: K20901000006-09E0100-00610) and the Seoul R&BD Program (10919).

References

[1] Walters DA, Ericson LM, Casavant MJ, Liu J, Colbert DT, Smith KA, et al. Elastic strain of freely suspended single-wall carbon nanotube ropes. Appl Phys Lett. 1999;74(25):3803-5.

[2] Tombler TW, Zhou C, Alexseyev L, Kong J, Dai H, Liu L, et al. Reversible electromechanical characteristics of carbon nanotubes under local-probe manipulation. Nature. 2000;405(6788):769-72.

[3] Kim G-T, Gu G, Waizmann U, Roth S. Simple method to prepare individual suspended nanofibers. Appl Phys Lett. 2002;80(10):1815-7.

[4] Kobayashi Y, Yamashita T, Ueno Y, Niwa O, Homma Y, Ogino T. Extremely intense Raman signals from single-walled carbon nanotubes suspended between Si nanopillars. Chem Phys Lett. 2004;386(1-3):153-7.

[5] Rueckes T, Kim K, Joselevich E, Tseng GY, Cheung C-L, Lieber CM. Carbon Nanotube-Based Nonvolatile Random Access Memory for Molecular Computing. Science. 2000;289(5476):94-7.

[6] Dai H. Carbon Nanotubes: Synthesis, Integration, and Properties. Acc Chem Res. 2002;35(12):1035-44.

[7] Cassell AM, Franklin NR, Tombler TW, Chan EM, Han J, Dai H. Directed Growth of Free-StandingSingle-Walled Carbon Nanotubes. J Am Chem Soc. 1999;121(34):7975-6.

[8] Franklin NR, Wang Q, Tombler TW, Javey A, Shim M, Dai H. Integration of suspended carbon nanotube arrays into electronic devices and electromechanical systems. Appl Phys Lett. 2002;81(5):913-5.

[9] Khakani MAE, Yi JH, Aïssa B. Localized growth of suspended SWCNTs by means of an "all-laser" process and their direct integration into nanoelectronic devices. IEEE Trans Nanotechnol. 2006;5(3):237-41.

[10] Abrams ZR, Ioffe Z, Tsukernik A, Cheshnovsky O, Hanein Y. A Complete Scheme for Creating Predefined Networks of Individual Carbon Nanotubes. Nano Lett. 2007;7(9):2666-71.

[11] Oh BS, Min Y-S, Bae EJ, Park W, Kim YK. Fabrication and characterization of suspended single-walled carbon nanotubes. Solid State Commun. 2006;139(4):186-90.

[12] Lee Y-H, Lee J-H, Noh J-Y. One-step grown suspended n-type semiconducting single wall carbon nanotube field effect transistors with carbon nanotube electrodes. Appl Phys Lett. 2008;92(4):043110-3.

[13] Jung YJ, Homma Y, Ogino T, Kobayashi Y, Takagi D, Wei B, et al. High-Density, Large-Area Single-Walled Carbon Nanotube Networks on Nanoscale Patterned Substrates. J Phys Chem B. 2003;107(28):6859-64.

[14] Iwasaki T, Morikane R, Edura T, Tokuda M, Tsutsui K, Wada Y, et al. Growth of dense single-walled carbon nanotubes in nano-sized silicon dioxide holes for future microelectronics. Carbon. 2007;45(12):2351-5.

[15] Gras R, Duvail JL, Min T, Dubosc M, Tessier PY, Cagnon L, et al. Template synthesis of carbon nanotubes from porous alumina matrix on silicon. Microelectron Eng. 2006 2006/12//;83(11-12):2432-6.

[16] Claussen JC, Franklin AD, ul Haque A, Porterfield DM, Fisher TS. Electrochemical Biosensor of Nanocube-Augmented Carbon Nanotube Networks. ACS Nano. 2009;3(1):37-44.

[17] An Y-H, Song S. Fabrication of a CNT filter for a microdialysis chip. Mol Cell Toxicol. 2006;2(4):279-84.

[18] Blow N. Microfluidics: the great divide. Nat Meth. 2009;6(9):683-6.

[19] Srivastava A, Srivastava ON, Talapatra S, Vajtai R, Ajayan PM. Carbon nanotube filters. Nat Mater. 2004;3(9):610-4.

[20] Brady-Estévez AS, Kang S, Elimelech M. A single-walled-carbon-nanotube filter for removal of viral and bacterial pathogens. Small. 2008;4(4):481-4.

[21] Ghosh S, Sood AK, Kumar N. Carbon nanotube flow sensors. Science. 2003 February 14, 2003;299(5609):1042-4.

[22] Homma Y, Yamashita T, Kobayashi Y, Ogino T. Interconnection of nanostructures using carbon nanotubes. Physica B. 2002;323(1-4):122-3.

[23] Searson PC, Macaulay JM. The fabrication of porous silicon structures. Nanotechnol. 1992;3(4):188-91.

[24] Yang HJ, Song HJ, Shin HJ, Choi HC. A rapid synthesis of iron phosphate nanoparticles via surface-mediated spontaneous reaction for the growth of high-yield, single-walled carbon nanotubes. Langmuir. 2005;21(20):9098-102.

[25] Lee TJ, Seo J, Lee H. Vertically aligned growth of single-walled carbon nanotubes on Fe-Mo/MgO/Si substrate prepared by using a dipping method combined with an UV-ozone treatment. J Korean Phys Soc. 2008;53(6):3236-40.

[26] Cantoro M, Hofmann S, Pisana S, Scardaci V, Parvez A, Ducati C, et al. Catalytic Chemical Vapor Deposition of Single-Wall Carbon Nanotubes at Low Temperatures. Nano Lett. 2006;6(6):1107-12.

[27] Homma Y, Kobayashi Y, Ogino T, Yamashita T. Growth of suspended carbon nanotube networks on 100-nm-scale silicon pillars. Appl Phys Lett. 2002;81(12):2261-3.

[28] Homma Y, Takagi D, Kobayashi Y. Suspended architecture formation process of single-walled carbon nanotubes. Appl Phys Lett. 2006;88(2):023115-3.

[29] Franklin NR, Dai H. An enhanced CVD approach to extensive nanotube networks with directionality. Adv Mater. 2000;12(12):890-4.

[30] Sauvajol JL, Anglaret E, Rols S, Alvarez L. Phonons in single wall carbon nanotube bundles. Carbon. 2002;40(10):1697-714.

[31] Lee TJ, Lee H. Ultraviolet irradiated ozone treatment of a metal catalyst for the large-scale synthesis of single-walled carbon nanotubes with small, uniform diameters. Carbon. 2008;46(11):1443-9.

[32] Kataura H, Kumazawa Y, Maniwa Y, Umezu I, Suzuki S, Ohtsuka Y, et al. Optical properties of single-wall carbon nanotubes. Syn Met. 1999;103(1-3):2555-8.

The 20th International Conference on ME&D

<http://www.aspbs.com/jnn>

REFEREE'S REPORT

Code no.: M-150

Author: Hyunsook Kim[a], Tae Jae Lee[b], Somin Kim[a] and Haiwon Lee

Title: **Modification of Silicon Substrate using Low-Energy Proton Beam for Selective Growth of CNTs**

Recommendations and comments should be sent within 2 weeks to the Editor from whom you received the Manuscript. Please type this report and return to the editorial office through e-mail <secretary-med@sogang.ac.kr>. Extra sheets of detailed comments should be typed in triplicate on paper that does not reveal your identity or affiliation. Any corrections or remarks inserted in the manuscript should be made in pencil. Any question, please contact, phone number : 82-2-705-7869, Ms. Ji-Won Han, Secretary)

Reviewer,

Extra sheets of detailed comments should be typed on paper that does not reveal your identity or affiliation, this document can then be uploaded as a separate attachment.

For each question below, please place an x in the appropriate space:

1. Is the subject matter suitable for publication in **Journal of Nano Science and Nano Technology**?

   YES _√_ NO __

2. Is the paper acceptable in its present form? YES __ NO __

   Is the paper acceptable with major revision? YES __ NO __

   Is the paper acceptable with minor revision? YES _√_ NO __

   Should the paper be rejected? YES __ NO __

3. Is the paper a new and original contribution? YES _√_ NO __

4. Is the title appropriate and adequate? YES _√_ NO __

5. Is the abstract adequate and informative? YES __ NO √__

6. Is the paper clearly presented and well organized? YES _√_ NO __

7. Are the conclusions sound and justified? YES __ NO _√_

8. Does the paper give adequate references to related and recent work? YES _√_ NO __

9. Are the illustrations and tables all necessary and adequate? YES _√_ NO __

10. Does the paper contain material that might well be omitted? YES _√_ NO __

11. Does this paper include timely very urgent subjects and substances ? YES _√_ NO __

12. Is the English good enough to be published ? YES _√_ NO __

Please list further comments or specific suggestions below or as a separate attachment.

<Referee's comment>

This paper need more clear abstract containing specific results. The conclusions also need more specific data.

▶ Authors would like to thank reviewers for keen comments. Authors were revised the abstract and conclusions.

[abstract]

A 3 keV low-energy proton beam was used to irradiate a silicon substrate for selective modification. The irradiated silicon substrate was covered with a silicon oxide layer of about 60 ~ 70 Å due to the incorporation of oxygen molecules after exposure to ambient air. To confirm the chemical properties of the silicon oxide layer, the triangular oxide pattern was fabricated by nanosphere lithography. The height of silicon oxide pattern was increased about 15 Å after removing the native silicon oxide layer on non-proton beam-irradiated silicon substrate by using HF solution. The water contact angle was measured on silicon substrates with various functional surface groups. The proton beam irradiated silicon oxide layer containing the Si-O-p surface group is more hydrophilic than the native silicon oxide removed silicon surface with Si-H surface group. The silicon oxide layer produced by the proton beam was highly resistant to HF treatment which typically used to remove the silicon oxide on a substrate. For the selective growth of carbon nanotubes (CNTs), the silicon oxide pattern was easily fabricated via proton beam irradiation when the silicon substrate was covered with a shadow mask. The Fe-Mo bimetallic catalysts for the growth of CNTs were adsorbed onto the silicon oxide layer, which is more hydrophilic than the silicon surface. The CNTs were grown on the patterned substrate using a chemical vapor deposition method, and it was confirmed by scanning electron microscopy.

[conclusion]

In this study, we demonstrated a basic technique for using low-energy ion beam lithography to modify a silicon substrate. The silicon substrate was partially modified by proton beam irradiation using a shadow mask without other materials or additional processes for growing CNTs on a desired area. The chemical etching process for removing the native oxide did not affect the silicon oxide layer formed by the proton beam, which had a different surface property than the base silicon surface. Also, the lower water contact angle was obtained on the Si-O-Pr surface than the native silicon oxide removed silicon substrate. The Fe-Mo bimetallic catalysts were well adsorbed onto the Si-O-Pr modified silicon oxide layer, preparing them for growth of CNTs. CNTs were selectively grown on the silicon oxide patterned substrate.

Modification of Silicon Substrate using Low-Energy Proton Beam for Selective Growth of CNTs

Hyunsook Kim[1], Tae Jae Lee[2], Somin Kim[1] and Haiwon Lee[1,2*]

[1]*Department of Chemistry, Hanyang University, Seoul 133-791, Korea*
[2]*Institute of Nano Science and Technology (INST), Hanyang University, Seoul 133-791, Korea*

A 3 keV low-energy proton beam was used to irradiate a silicon substrate for selective modification. The water contact angle measurement, chemical etching test with HF and the auger electron spectroscopy were used to investigate the chemical properties and the material composition of the proton beam-irradiated silicon substrate. The proton beam-irradiated silicon substrate was covered with a silicon oxide layer of about 60 ~ 70 Å due to the incorporation of oxygen molecules after exposure to ambient air. The silicon oxide layer produced by the proton beam was highly resistant to HF treatment which typically used to remove the silicon oxide on a substrate, and the surface of it was more hydrophilic than the native silicon oxide removed silicon surface with Si-H surface group. For the selective growth of carbon nanotubes (CNTs), the silicon oxide pattern was easily fabricated via proton beam irradiation when the silicon substrate was covered with a shadow mask. The Fe-Mo bimetallic catalysts for the growth of CNTs were adsorbed onto the silicon oxide layer, which is more hydrophilic than the silicon surface. The CNTs were grown on the patterned substrate using a chemical vapor deposition method, and it was confirmed by scanning electron microscopy.

Keyword: Low-energy proton beam, Silicon oxide pattern, Carbon nanotubes

1. Introduction

Low-energy ion beam irradiation has been used for surface modification of materials because of its ability to change the mechanical, chemical, and physical properties of materials.[1,2] Several authors have reported the characteristics of ion-beam irradiated polymers[3,4], organos ilnane self-assembled monolayers[5], and semiconductor materials[6-8]. In addition, it has been reported that low-energy ion beams are a useful tool for depositing a dielectric layer, such as SiO_2, SiGe, GeO_2, and GaAs oxide, onto various substrates.[9] Fossum *et al.* reported the growth of a silicon oxide layer with the use of oxygen-containing, low-energy ion beam irradiation on a silicon substrate.[10,11] They investigated the effect of ion dose, ion energy, and temperature on the thickness of the oxide film, which was limited to 40 - 60Å due to the competing processes of implantation and sputtering. In a previous study, we also investigated the effect of low-energy Ar-ion beams on a silicon substrate.[12,13] The silicon oxide layer formed after Ar-ion beam irradiation was due to the incorporation of oxygen molecules when the substrate was exposed to ambient air.

Carbon nanotubes (CNTs) have been studied due to their electrical, chemical and mechanical properties. It is imperative that CNTs are grown directly on the desirable site to ensure proper device application, and various methods such as atomic force microscope (AFM) anodization lithography[14], dip-pen lithography[15], micro-contact printing[16], nanoimprint lithography[17], and e-beam lithography[18] have all been used to grow CNTs on various surfaces. These techniques have also been proposed for use in applying CNTs to field emission displays;[19,20] however the complicated process of catalyst patterning is needed to grow the CNTs on the required large surface area. Here, we propose a simple method for the selective growth of the CNTs on a silicon substrate.

In this study, the effect of low-energy proton beams, which is one of methods for selective modification of a silicon substrate, was investigated, as the chemical and physical properties of a silicon oxide layer formed by proton beams have not yet been reported. We found that the chemical etching

process for removal of the native oxide layer did not etch the silicon oxide layer formed by the proton beam. The silicon oxide pattern was fabricated using a shadow mask, and was subsequently applied for the selective growth of CNTs.

2. Experiment

2.1. Materials

Methanol, tetrahydrofuran (THF), ethanol, isopropyl alcohol (IPA), acetone, and molybdenum inductively coupled plasma (ICP) spectrometry standard solution (10,000 μg/ml Mo in H_2O) were obtained from Aldrich. All solvents were high performance liquid chromatography grade. $Fe(NO_3)_3 \cdot 9H_2O$ (assay min. 98.0 %), hydrofluoric acid (HF) (assay min. 50 %), hydrogen peroxide (H_2O_2) (assay min. 34 %), and sulfuric acid (H_2SO_4) (assay min. 95 %) were purchased from Junsei. A p-type silicon wafer (100) was obtained from the Silicon Technology Corporation. Polystyrene (PS) nanospheres with a 400 nm diameter were purchased from Bangs Lab (Fisher, IN, USA).

2.2. Characterization of silicon oxide formed by a proton beam

Figure 1 shows the experimental process for the selective modification of a silicon substrate using nanosphere lithography. A PS nanosphere array was placed onto the silicon substrate by the drop-coating method using 20 μl of the nanosphere solution diluted by mixing with a solution of methanol and DI water (Fig. 1a). A 3 keV low-energy proton beam with a fluence of 1×10^{16} ions/cm^2 was irradiated onto the silicon substrate in a high-vacuum chamber with a base pressure of 1.5×10^{-6} Torr (Fig. 1b). After irradiation with the proton beam, the PS nanospheres were removed using THF solvent (Fig. 1c). The substrate was treated with a 1.0% HF solution diluted with DI water (Fig. 1d). The height variation of the silicon oxide layer after HF treatment was measured using atomic force microscopy (AFM) (Nanoscope IIIa, Digital Instruments, CA). AFM was operated in the tapping mode with Al backside-coated silicon tips, which had a resonance frequency of 320 kHz and a radius curvature of less than 10 nm (Nanoworld).

Composition of the silicon oxide layer on the substrate was determined by auger electron spectroscopy (AES) (PHI 680 Auger Nanoprobe, Physical Electronics.) AES was performed under an electron beam at 10 kV and 10 nA. The water contact angle on the silicon surface was measured using a KRÜSS model FM 40 goniometer with various functional groups including Si-OH, Si-H, Si-O-Si, and Si-O-Pr. The Si-OH functional group was generated by treatment with a piranha solution (H_2O_2:H_2SO_4 = 3:7 v/v %). The Si-H surface group was generated on the silicon substrate by treatment with the HF solution. The Si-O-Si surface functional groups of the native oxide layer were cleaned with acetone, IPA, and DI water. The Si-O-Pr is a virtual surface functional group of the silicon oxide layer formed by the proton beam.

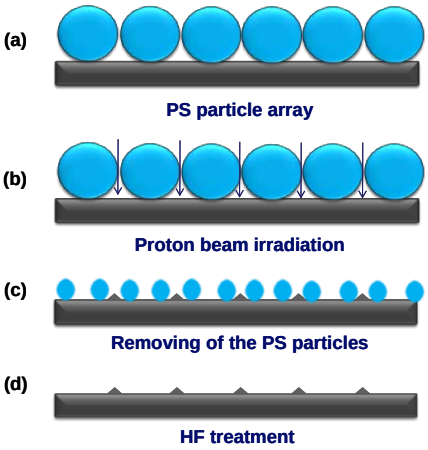

Figure 1. The fabrication process of silicon oxide structures using nanosphere lithography and proton beams.

2.3. Selective growth of CNTs on the oxide pattern

The HF-treated substrate coated with the silicon oxide pattern was immersed in a 0.01M Fe-Mo bimetallic catalyst solution in ethanol for two hr. The Fe-Mo bimetallic catalyst solution was prepared using $Fe(NO_3)_3 \cdot 9H_2O$ and a molybdenum ICP standard solution. The catalyst-adsorbed substrates were inserted into the center of a quartz tube reactor. The CNTs were synthesized in a horizontal quartz tube reactor at less than 1.0×10^{-2} Torr and about 800°C. A 500 sccm NH_3 gas flow rate was used for ten min at 800°C to reduce the metal oxide onto the metal catalyst. For growth of the CNTs, 200 sccm C_2H_2 gas was added into the reactor for ten min. After synthesis of the CNTs, the reactor was cooled to room temperature.[21] Scanning electron microscopy (SEM) (S-4700, Hitachi) was used to analyze the selective CNTs grown on the silicon oxide pattern.

3. Results and Discussion

Figure 2 shows AFM images of the silicon oxide pattern produced by proton beam irradiation and the height of oxide dots according to etch time with HF.

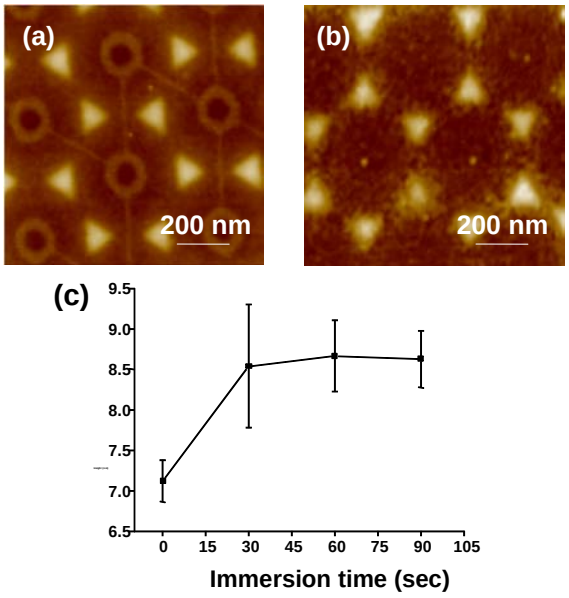

Figure 2. AFM images of silicon oxide structures fabricated by proton beam irradiation using a PS array; (a) after removal of the PS nanospheres and (b) after HF treatment. (c) The height of the silicon oxide layer vs. HF etch time of the native oxide layer.

After removal of the PS nanospheres, the polymer ring pattern remained in the center of the hexagonal oxide dot configuration (Fig. 2a). This pattern was a result of the scattered proton beam affecting the PS nanospheres through a radical reaction with the polycyclic structure.[1] The polymer rings were cleared by HF treatment as shown in Fig. 2b. Figure 2c shows height variations in the silicon oxide dots according to the total HF etch time of the native oxide layer. The height variation of the silicon oxide dots was saturated at about 15 Å, which is the thickness of the native oxide layer on a bare silicon substrate.[22] This indicates that the native oxide layer was removed by the HF solution, but the silicon oxide formed by the proton beam was not influenced by the HF treatment. Also, the silicon oxide dots had a strikingly different structure relative to that of the native oxide.

Figure 3 shows the auger depth profiles of the bare silicon and proton-beam irradiated silicon substrates. The initial atomic ratio of oxygen for the bare silicon substrate was 50%; however, the atomic ratio of oxygen for the proton-beam irradiated silicon substrate was higher than that of the bare silicon. This indicates that the proton beam caused damage to the Si–Si chemical bond, and that the resulting unstable Si atoms reacted with oxygen either from the ambient water or air, to form a more stable chemical state. Oxygen was detected to about 30 Å and 60 Å depths on the bare silicon and proton-beam

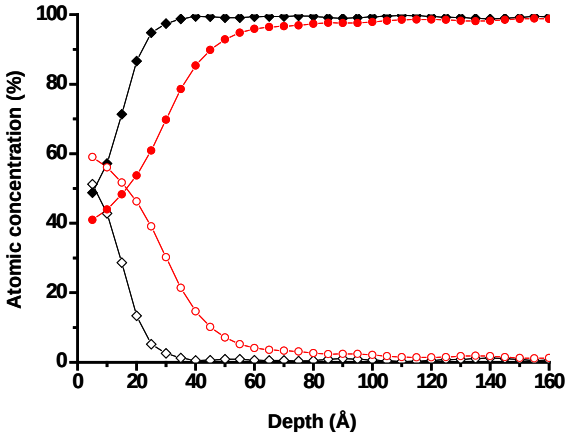

Figure 3. AES depth profiles of the bare silicon substrate (-◆- and -◇-) and the proton-beam irradiated silicon substrate (-●- and -○-). Profile data for two components of silicon (-◆-and-●-) and oxygen (-◇- and -○-) on the sample are shown.

irradiated silicon substrates, respectively (Fig. 2). This indicates that the proton beam penetrated through the silicon substrate, allowing the oxygen to diffuse into the damaged silicon layer.

The physical property of the surface was characterized by measuring the water contact angles on both silicon surfaces. Figure 4 shows the values of the water contact angles on the four surfaces. The water contact angle of the Si-OH modified surface was below 7°, due to the extreme hydrophilic property of this surface. The mean contact angle between the water and the Si-O-Si was about 28°. After removing the native oxide by HF treatment, the water contact angle of the Si-H surface was increased to about 80°[23], which is comparable to the contact angle of 68° measured on the Si-O-Pr surface. These data indicate that the Si-O-Pr-modified surface is more hydrophilic than the Si-H surface, and that the physical properties between the Si-O-Si and Si-O-Pr

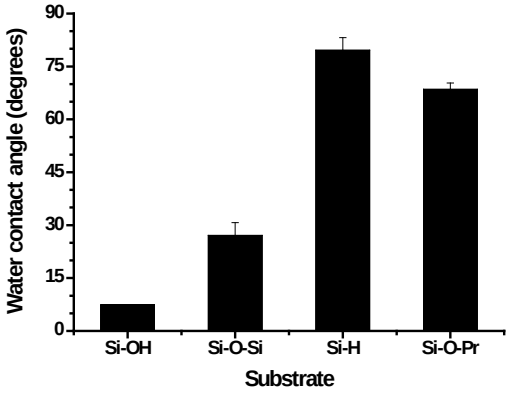

Figure 4. Water contact angles for various silicon surfaces.

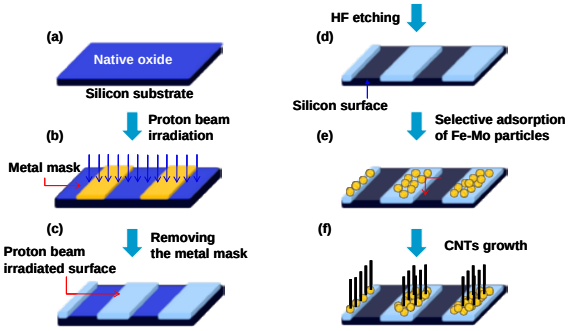

Figure 5. Fabrication of the silicon oxide pattern for the selective growth of CNTs.

surfaces are different.

Figure 5 shows the experimental process for fabricating the oxide pattern for the selective growth of CNTs. The proton beam was directly irradiated onto the silicon substrate, which was covered with a shadow mask as shown in Figs. 5a and 5b. The beam-irradiated substrate was treated with a HF solution as previously described (Figs. 5c and 5d). When the substrate was put into the Fe-Mo bimetallic solution, the Fe-Mo particles adsorbed to the more hydrophilic surface (Fig. 5e). Figure 6 shows the AFM images of the Fe-Mo adsorbed surfaces of both the silicon oxide layer and the bare silicon surface. The density of Fe-Mo particles on the silicon oxide layer was higher than that on the silicon surface because the adsorption of metal ions depends upon the hydrophilic or hydrophobic property of the surface. These results are similar to those of Moon *et al.* that reported the adsorption rate of metal ions was increased on hydrophilic compared to hydrophobic surfaces.[24]

Figure 7a shows SEM images of the oxide patterns corresponding to Fig. 5c. The pitch of the pattern was 200 μm, which consisted of the 50 μm between the oxide patterns (dark area) and the pattern width of 150 μm (bright area). The SEM image of selectively grown CNTs was obtained at the interface

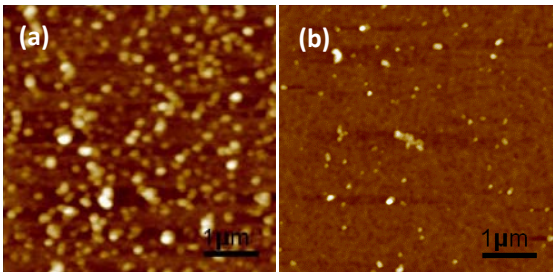

Figure 6. AFM images after Fe-Mo adsorption onto a substrate with a silicon oxide pattern; (a) silicon oxide and (b) silicon surface.

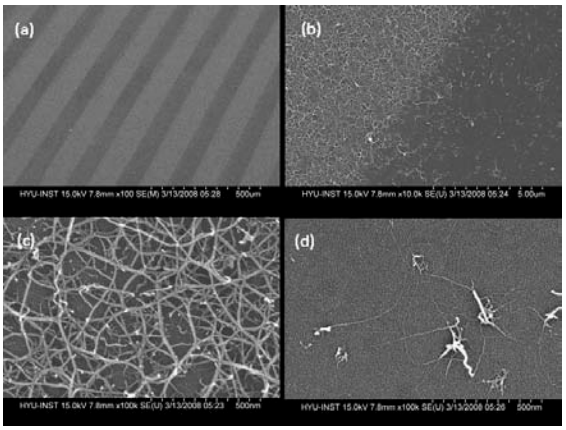

Figure 7. SEM images after growth of CNTs on the silicon oxide pattern; (a) silicon oxide pattern before CNT growth, (b) interface image between the silicon oxide layer and the silicon surface after CNT growth. Enlarged images of CNTs on the (c) silicon oxide layer and (d) silicon surface.

between the silicon oxide layer and silicon surface as shown in Fig. 7b. The density of CNTs on the silicon oxide layer was higher than that of the silicon surface because the density of CNTs depends on the number of Fe-Mo particles. Enlarged images of CNTs on the silicon oxide layer (Fig 7c) and on the silicon surface (Fig 7d) are shown.

4. Conclusion

In this study, we demonstrated a basic technique for using low-energy ion beam lithography to modify a silicon substrate. The silicon substrate was partially modified by proton beam irradiation using a shadow mask. The chemical etching process for removing the native oxide did not affect the silicon oxide layer formed by the proton beam, which had a different surface property than the base silicon surface. Also, the lower water contact angle was obtained on the Si-O-Pr surface than the native silicon oxide removed silicon substrate. The Fe-Mo bimetallic catalysts were well adsorbed onto the Si-O-Pr modified silicon oxide layer, preparing them for growth of CNTs. CNTs were selectively grown on the silicon oxide patterned substrate.

Acknowledgments: This work was supported by the National Program for Tera-Level Nanodevices of the Ministry of Science and Technology as one of the 21st Century Frontier Programs (TND) and the Korea Foundation for International Cooperation of Science

& Technology (KICOS) through a grant provided by the Korean Ministry of Science & Technology (MOST) in No. k20501000002-07-E0100-00210, and partially supported by the Seoul R&BD Program (10919). This work was supported by the International Research & Development Program of the National Research Foundation of Korea (NRF) funded by the MEST of Korea (Grant number: K20901000006-09E0100-00610) and the Seoul R&BD Program (10919). This work was supported by a grant (08K1501-02011) from the 'Center fo r Nanostructured Materials Technology' under the '21st Century Frontier R&D Programs' of the Mi nistry of Education, Science and Technology (MEST) of Korea, and by a grant (AOARD-08-40 04) from AFOSR/AOARD of USA.

References

1. M. E. Martíez-Pardo, J. Cardoso, H. Vázquez and M. Aguilar, *Nucl. Instrum. Meth. B* 140 , 325 (**1998**).
2. H. H. Brongersma, M. Draxler, M. Ridder and P. Bauer, *Surf. Sci. Rep.* 62, 63 (**2007**).
3. M. Komuro, N. Atoda and H. Kawakatsu, *J. Electrochem. Soc.* 126, 483 (**1979**).
4. T. M. Hall, A. Wagner and L. F. Thompson, *J. Appl. Phys.* 53, 3997 (**1982**).
5. E. T. Ada, L. Hanley, S. Etchin, J. Melngailis, W. J. Dressick, M. S. Chen and J. M. Calvert, *J. Vac. Sci. Technol. B* 13, 2189 (**1995**).
6. T. K. Chini, D. P. Datta, S. Facsko and A. Mucklich, *Appl. Phys. Lett.* 92, 101919 (**2008**).
7. R. Gago, L. Vazquez, R. Cuerno, M. Varela, C. Ballesteros and J. M. Albella, *Appl. Phys. Lett.* 78, 3316 (**2001**).
8. S. K. Mohanta, R. K. Soni, S. Tripathy and S. J. Chua, *Appl. Phys. Lett.* 88, 043101 (**2006**).
9. O. Vancauwenberghe, O. C. Hellman, N. Herbots and W. J. Tan, *Appl. Phys. Lett.* 59, 2031 (**1991**).
10. S. S. Todorov and E. R. Fossum, *Appl. Phys. Lett.* 52, 48 (**1988**).
11. S. S. Todorov and E. R. Fossum, *J. Vac. Sci. Technol. B* 6, 466 (**1988**).
12. S. K. Kim, H. Kim and H. Lee, *J. Korean Phys. Soc.* 52, 930 (**2008**).
13. H. Kim, S. K. Kim, K. R. Kim and H. Lee, *Ultramicroscopy* 334, 161 (**2009**).
14. C. C. Chiu, M. Yoshimura and K. Ueda, *Diam. Relat. Mater.* 18, 355 (**2009**).
15. B. Li, C. F. Goh, X. Zhou, G. Lu, H. Tantang, Y. Chen, C. Xue, F. Y. C. Boey, and H. Zhang, *Adv. Mater.* 20, 4873 (**2008**).
16. S. Huang, A. W. H. Mau, T. W. Turney, P. A. White and L. Dai, *J. Phys. Chem. B* 104, 2193 (**2000**).
17. S. M. C. Vieira, K. B. K. Teo, W. I. Milne, O. Groning, L. Gangloff, E. Minoux and P. Legagneux, *Appl. Phys. Lett.* 89, 022111 (**2006**).
18. K. C. Park, J. H. Ryu, K. S. Kim, Y. Y. Yu and J. Jang, *J. Vac. Sci. Technol. B* 25, 1261 (**2007**).
19. C. C. Chiu, T. Y. Tsai and N. H. Tai, *Nanotechnology* 17, 2840 (**2006**).
20. S. J. Oh, Y. Cheng, J. Zhang, H. Shimoda and O. Zhou, *Appl. Phys. Lett.* 82, 2521 (**2003**).
21. T. J. Lee, *J. Korean Phys. Soc.* 53, 3236 (**2008**).
22. M. Morita, T. Ohmi, E. Hasegawa, M. Kawakami and M. Ohwada, *J. Appl. Phys.* 68, 1272 (**1990**).
23. G. Gould and E. A. Irene, *J. Electrochem. Soc.* 135, 1535 (**1988**).
24. J. Moon, T. Kang, S. Oh, S. Hong and J. Yi, *J. Colloid Interf. Sci.* 298, 543 (**2006**).